# Leg placement control based on passive dynamics of a 3D walking model

Haris Organtzidis

A dissertation submitted in partial fulfilment of the requirements of the University of the West of England, Bristol for the Degree of Master of Science
MSc Robotics

August 2017

This study was completed for the MSc in Robotics the University of the West of England, Bristol. The work is my own. Where the work of others is used or drawn on it is attributed.

Haris Organtzidis

Word count : 12459

I would like to thank Dr JF Burn for our discussions and my family and Elena for their continuous support.

# Abstract

The present work is an investigation of the stability of an abstract model for walking, comprising of a point mass and two massless spring legs, when open-loop strategies are employed to adjust the position of each leg before ground contact. This model is a 3D extension of established models in literature. Some of the most successful state-of-the-art robotics applications have utilised similar models as the basis of walking machines. Recent experiments have produced evidence supporting the hypothesis that the control of leg placement in human walking might be based on similar open-loop strategies as the ones tested on the model. The stability analysis of the proposed model was conducted using 10 such strategies with the aims of introducing guidelines for the design and control of robust walking robots that additionally minimise energy expenditure and determining the extent at which humans rely on passive dynamics of their body to attain stability while walking. The results indicated two successful strategies, with one exhibiting superior robustness. The caveat of both strategies was their inability to maintain a desired walking direction under perturbations. However, a close similarity was found between the hypothesised choice of step width from the experimental literature and the equivalent equation of the model. This constitutes an analytical support of the experimental evidence, implying that the control of human walking could be at least partially explained by an abstract model with simple control. Regarding applications to walking robots, the most robust strategy did not require precise leg placement to achieve asymptotic stability while yielding large areas of stable walking. This work encourages a more thorough investigation of the model's phase space and design parameters, such as leg stiffness, using this strategy, in order to fully determine the amount of allowable deviations from precise leg control and margins of stability under perturbations.

# Contents

# Chapter 1

# Introduction

The field of biologically inspired robotics has been attracting increased attention in recent years (Ijspeert (2014)). The motivation on the field is driven by the large number of potential applications for artificial systems that are able to move like human in human-made environments or negotiate unstructured natural terrain as animals do. Some examples include assistive humanoids, prosthetics, agriculture, search and rescue missions and forming test-beds to replace animals in experiments ((Kajita and Espiau, 2008, p. 1395-1418), Ijspeert (2014)). The design of legged robots ((Kajita and Espiau, 2008, p. 361-387) is one of the subfields of biologically inspired robotics that have been directly influenced by terrestrial animals, since the early work of Raibert (1986) on hopping and running machines. The inspiration drawn from animals comprises of key features of their locomotion, such as stability, energy efficiency, manoeuvrability and movement in different gaits (Holmes et al. (2006)). The present work was focused on bipedal walking systems and the intersection between stability and energy efficiency.

Stability is arguably the feature with the highest priority during the process of controlling locomotion. Ferris et al. (1999) noted that human runners expended energy in order to adjust the leg stiffness during the first step on a new compliant surface. This adjustment was made in order to produce smooth centre of mass trajectories that ensure stability while following the principle of a mass bouncing on a linear spring. Birn-Jeffery et al. (2014) observed similar results for guinea fowls while negotiating a single obstacle with a pronounced priority given to energy efficiency. Walking inherently includes an instability, as the centre of mass oscillates from side to side while it moves along a chosen direction. Perturbations typically present in real world scenarios in the form of lateral forces or uneven terrain add to the system's inherent instability. Numerous approaches to design and stability control have been proposed and implemented on

walking robots, with an increasing focus on the way animals manage to retain their stability while moving through various substrates (Zhou and Bi (2012)). However, the exact control law that bipeds utilise to remain stable while walking has not yet been determined (Pfeiffer and Inoue (2007)). Recent experimental studies have presented evidence that simple leg placement strategies might be employed by humans to attain stability while walking (Hof et al. (2007), Wang and Srinivasan (2014)).

The word *simple* was used in the present report to describe open-loop leg placement strategies that rely on the body design and structure rather than active control that originates in the neuromuscular system. The former minimises sensory and decision making requirements, while exploiting the passive dynamics of the body (Blickhan et al. (2007)). The latter has been the standard approach for years and it has led to implementations on versatile robots that expend large amounts of energy and time in their effort to compute and apply a detailed control strategy (Holmes et al. (2006) for a review). Simple leg strategies are based on the passive dynamics of a mathematical model, which is the abstract basis for the design of the actual robots. If a certain strategy leads to stable periodic walking of the model, then both the strategy and the model morphology can be used as an abstract basis for the development of complex walking robots.

An inverted pendulum, with a concentrated mass to represent the centre of mass, has been used to model walking, initiated by the work of Cavagna and Margaria (1966). Hurmuzlu et al. (2004) presented an overview of robotics applications based on this model. However, recent work by Geyer et al. (2006) has shown that the spring-mass model, typically used for running and first proposed by Blickhan (1989), can better predict the dynamics and energy exchanges during walking in humans. Moreover, it introduced the double support phase during each step, an essential part of walking where the weight load is gradually transferred from the trail to the leading leg as both of them are in contact with the ground. The present work extended the bipedal model to the 3D case, in order better to trade-off between simplicity and realistic simulation. Thus, the model matched real-world walking in terms of spatial dimensions. It is therefore more meaningful to evaluate leg placement strategies on the proposed model in order to produce guidelines for robotic applications that aim to replicate human locomotion.

Additionally, the model was used to test the hypothesis from the experimental literature of whether stability in walking could emerge from simple control laws. If the 3D bipedal spring-mass model could capture the walking behaviour exhibited by humans while utilizsng a simple leg strategy, it would indicate that the inherent leg compliance is sufficient for stability without any neural processing. Consequently, further insight may

be gained about the origin of locomotion control in humans. It could lead to a novel, more representative *template* model for walking, an abstract basis from where more complex *anchor* models can be developed to investigate detailed features of human movement or to accommodate model-based control techniques implemented in legged robots (Full and Koditschek (1999)).

No work has been done on investigating the stability of a 3D bipedal spring-mass model. This investigation revolved around simulating walking steps of the proposed hybrid dynamical system that describes the dynamics of walking. When the complexity of the model allowed it, formal mathematical techniques were used to find periodic solutions of the hybrid system that corresponded to steady state walking. When assessing the robustness of the system under perturbations around its solution, analytical methods were unavailable and an intuitive computational approach was implemented, based on simulating a predetermined number of steps. This process was repeated for every potential simple leg strategy and consequently strategies that have exhibited stable walking were compared in terms of robustness and feasibility.

Summarising, the aims of the present work were to produce a stable system with minimal active control based on an abstract locomotion model and grant additional information about the control of stability in humans; whether it consists mainly of open-loop strategies dependent on the passive dynamics of the body or neuronal processes with sensorimotor coordination facilitated by the brain. The rest of the report is organised as follows : in Chapter 2 the relevant biomechanics and robotics literature is reviewed, Chapter 3 includes a detailed description of the mathematical model, the different leg strategies considered and the computational methods employed to assess their stability, in Chapter 4 the results of this investigation are presented and finally Chapter 5 consist of a discussion on the outcome of the project and some potential future extensions.

# Chapter 2

# Literature Review

The aim of the present work was to characterise the stability of an abstract mathematical model for walking driven by its inherent dynamics and simple leg placement strategies for each consequent step. This aim was motivated both by findings in the experimental biomechanics literature about the control of walking stability, advancements in the modelling literature on models that replicate locomotion and examples of strengths and limitations of state-of-the-art robots that employ either similar or entirely different approaches to control walking. The present literature review was an extension of an initial review submitted by the author for a coursework assignment of the Robotics Research Preparation unit of the MSc Robotics programme at the University of Bristol and direct quotation with citation of the coursework was used in this section when appropriate.

Walking dynamics were originally simulated by an inverted pendulum model. The energy exchanges between kinetic and gravitational potential energy were reported in Cavagna et al. (1977) for humans and walking birds. The inverted pendulum model predicted an ideal $100$% energy recovery, as the kinetic and gravitational energy oscillated out of phase, whereas the corresponding value measured in the experiments was $70$%. Despite of this discrepancy, the inverted pendulum model became the most popular model as an abstract basis for walking dynamics, termed the *template* model for walking (Full and Koditschek (1999)). Its broad applications range was rooted on its inherent simplicity and the work of McGeer (1990), who built passive walking machines that were able to walk down an incline by taking advantage of the $100$% energy exchange of the inverted pendulum model. These passive walkers were the most energy efficient realisable walking systems. Nevertheless, they were limited to walking downhill and lacked robustness under perturbations, whose direction did not coincide with the walking direction, as they were based on a 2D model.

Passive walking robots with added active control were able to compensate for the inherent instability that characterises 3D walking, while benefiting from the remarkable energy efficiency of the completely passive walkers of McGeer (1990). Collins et al. (2005) described three recent examples of bipedal robots that combine the passive dynamics principle of an inverted pendulum and some form of active control. The Cornell and Delft bipeds actuated the ankle to lift the leg off the ground and actively rotated the leg during its swing phase, strategies similar to those implemented by humans. These strategies led them to achieve humanlike walking gaits without any high-power and high-frequency actuators, that are not present in humans as well, thus supporting the argument that human walking is governed by similar simple control processes. ”Moreover, Cornell’s control strategy of trying to push off the stance leg just before the swing leg’s heel-strike resulted in high torque demand on the ankle motor and in high sensitivity of the push-off timing that could not be compensated. This highlighted the importance of the double support phase in walking, where push-off and heel-strike overlap and the weight load is transferred from one leg to the other with no severe energy penalties (Geyer et al. (2006)). Kuo (1999) extended McGeer’s planar walkers to 3D, by adding the roll angle (i.e rocking from side to side) in the inverted pendulum model. After comparing five control strategies, the authors concluded that controlling the lateral position of the foot was the most energy efficient strategy. The same model, with lateral foot placement implemented as the control law, was compared to experimental data of humans walking in Bauby and Kuo (2000), to show that it predicted the coupling between frontal and lateral foot placement more accurately than the model without active control. Additionally, the variance in lateral foot placement during experiments, which increased after deprivation of vision, indicated that this strategy was likely the result of visual or vestibular feedback control and its inherent noise, whereas frontal foot placement was facilitated by passive dynamics.” ((Organtzidis, 2017, p. 2-5))

”Hof et al. (2007), by conducting a walking experiment, including both healthy subjects and amputees, concluded that the centre of pressure, the point where the next foot contacts the ground, is kept at a fixed distance from the extrapolated centre of mass, which is the centre of mass with an added term proportional of centre of mass velocity. This result led to the formulation of the stepping strategy, a simple control law of walking by lateral foot placement, dependent upon centre of mass velocity. Although variance in lateral foot placement was also noted in Hof et al. (2007), it was not sufficient to disprove the hypothesis of constant distance between the centre of pressure and extrapolated centre of mass. In a following study (Hof et al. (2010)), the stepping strategy, along with an ankle strategy which accounts only for small lateral foot placement corrections, were tested in an experimental set-up that included human treadmill walking

and lateral perturbations in various gait phases. When the reaction time was sufficient, typically 300ms for the stepping and 200ms for the ankle strategy, both strategies were validated. Oddsson et al. (2004) perturbed the right foot of humans, during the middle of a step, forward or rearward diagonally by translating a platform. They verified that control of balance is regulated by adjusting the moment arm between the centre of mass and the stance leg to compensate for the disturbance torque, as the resulted step width changes were almost linearly scaled to the magnitude of the perturbation. This magnitude can be safely assumed to affect the centre of mass velocity relatively more than its position as the perturbation is brief (0.5 and 0.7 m/s for 5cm and 10cm platform translations respectively), similarly to Hof et al. (2010). Further support of the stepping strategy was provided in Wang and Srinivasan (2014), where data was collected from steady state walking. Linear relationships between next foot position and centre of mass position and velocity during different gait cycle phases were derived and it was shown that mainly the state of the centre of mass (i.e position and velocity) was responsible for lateral foot placement, even as early as the middle of a step. Finally, Vlutters et al. (2016) applied both lateral and anteroposterior perturbations with various magnitudes on walking subjects. A linear relation between foot placement and lateral centre of mass velocity emerged, in agreement with Hof et al. (2007). However, the changes in double support phase duration after perturbations observed in this study were not present in previous references. The authors argued that a model which incorporates a double support phase, like the bipedal spring-mass model would be more helpful in investigating balance control strategies during walking. It was evident from the above examples from the experimental literature that the velocity of the centre of mass was playing an important role in stable walking. The complete velocity vector could be captured by a 3D model of the dynamics of a point mass in place of the centre of mass position." ((Organtzidis, 2017, p. 2-5))

"Evidence of leg compliance during walking are increasing in the literature. Fukunaga et al. (2001) conducted an *in vivo* investigation of *gastrocnemius medialis* (GM), one of the major leg muscles and found that length changes during walking. It was shown that while the muscle contracts isometrically, its corresponding tendon behaves like a spring, executing a stretch - recoil cycle on each step. The authors mentioned that elastic energy storage along with the interchange between kinetic and gravitational potential energy of the inverted pendulum model were the two energy-saving mechanisms interacting during walking. This interaction was better depicted in the spring-mass model rather than in the inverted pendulum model. Additionally, Geyer et al. (2006), building on initial observations of Cavagna et al. (1977), showed that the bipedal spring-mass model predicted the vertical centre of mass oscillations, the ground reaction force pro-

file during each step, including during the double support phase, and the energy exchanges, more accurately than the inverted pendulum. Their model parameters are leg (spring) stiffness, leg angle and the conservative system energy. They argued that the bipedal spring-mass model unified the waking and running gaits and predicted additional stable gaits, with ground reaction force profiles not possible in human locomotion. Rummel et al. (2010) analysed this model with no active control in order to identify the range of spring stiffness values that allowed for stable walking. Solutions in the parameter space were found that exhibited both self-stability, the notion of attaining stability effortlessly (Blickhan et al. (2007)), and robustness to perturbations for a sufficient range of angles of attack even for the largest stiffness value, so that frontal leg adjustments before touch down were not necessary. This observation was in agreement with the assumption that frontal foot placement relied on passive dynamics, as noted above (Bauby and Kuo (2000)). The results also encompassed the case of high energy efficiency and low robustness of the passive walkers, when stiffness tended to infinity. ” ((Organtzidis, 2017, p. 2-5))

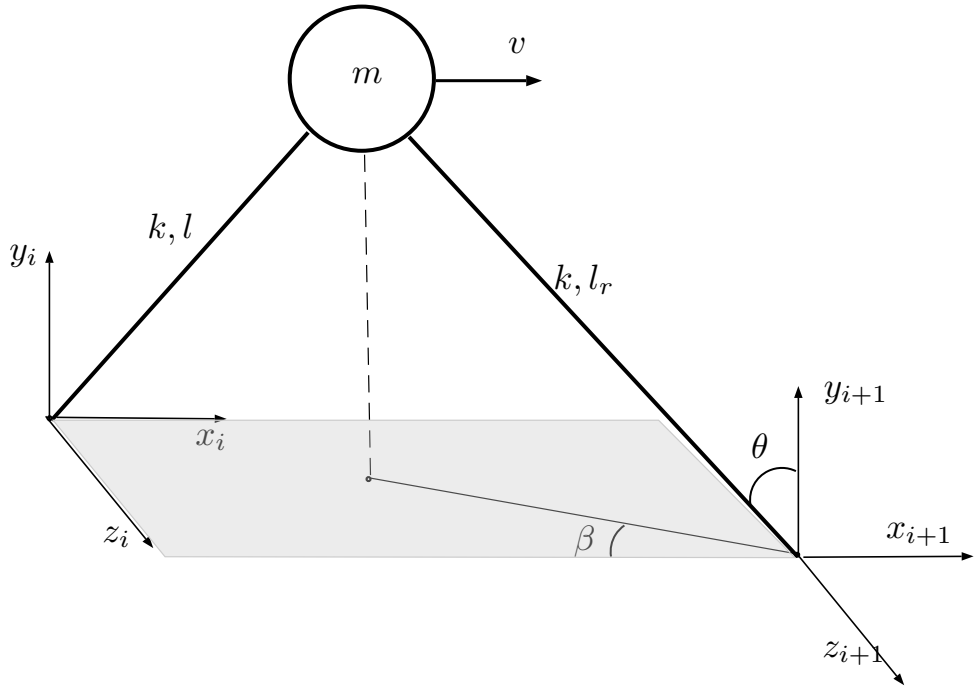


Figure 2.1: The 3D bipedal spring-mass model during right leg touch-down on the $i^{th}$ step

”There was an apparent agreement between walking experiments and the 2D bipedal spring-mass model about the significance of frontal leg placement ($\theta$ angle in Figure 2.1), as discussed in the two preceding paragraphs. The angle of attach for frontal placement of the leg did not have to be precisely controlled in order to attain stability, thus it could be claimed that stability relied on the compliance of the human leg that

was embedded in the model as well. Besides the accomplished asymptotic stability for a large range of angles of attack, Vejdani et al. (2015) proposed a leg strategy that controled the leg angle more precisely in order to achieve deadbeat control of the system, as it returned to its steady state in a minimum of two walking steps. The entirety of the relevant work was concerned with the 2D bipedal model, which can only describe a planar view of actual walking, commonly known as the *saggital* plane ($x, y$ plane in Figure 2.1), while ignoring the *horizontal plane* ($x, z$ plane in Figure 2.1), where lateral oscillations of the centre of mass occur. The lateral component of leg placement ($\beta$ angle in Figure 2.1), expressed on the *horizontal plane*, was the one assumed to rely on active control, as it was evident from the experimental literature discussed above. Thus it was more meaningful to use the 3D bipedal spring-mass model in an effort to determine whether a simple control law, comprising of a minimal active component and the passive leg dynamics, can lead to stable walking. The only published work on the 3D model was Maus and Seyfarth (2014), where stable walking was indeed achieved by actively controlling lateral leg placement using centre of mass velocity information. However, the aim of the study was to show that the model was able to predict the circular gait that disoriented or blind people exhibit, as they utilise body-centric information with no external references. There was no attempt to evaluate the robustness of the resulted stable solutions. Nevertheless, it was a successful first attempt to describe the complete 3D case of walking that was based on velocity information, the importance of which was highlighted by most experimental publications above. The successful strategy was one of the 6 proposed strategies in Peuker et al. (2012), where all of them were tested on a 3D spring-mass model for running. Although there is significant evidence that stability in running is firmly based on passive dynamics (Full and Koditschek (1999)), the proposed strategies are ideal candidates for the present case of 3D walking through simple control as they integrate only centre of mass position and velocity values in open-loop to attain stability." ((Organtzidis, 2017, p. 2-5))

"Robots incorporating springs have been built since the early stage of bio-inspiration in the field. Alexander (1990) proposed three uses of springs in robot design, while commenting on the energy efficiency achieved by the same uses in animals. One of them was the *pogo stick principle* which essentially resembled the spring-mass model. Raibert (1986) utilised this principle on a one-legged hopping and a quadruped robot. Since then, springs have been commonly used in robotics mainly to achieve running or hopping gaits. More recently though, successful examples of compliant legs in walking robots have been reported. Pratt et al. (2001) developed a virtual model control, where a variety of virtual components that also have a physical representation (e.g springs and dampers) were used as the control model, instead of the actual robot. This

method was implemented on the MIT Flamingo, a bipedal walker able to step over obstacles. The approach is adaptive, requiring the designer to formulate the appropriate virtual model for an application. A simpler approach was proposed by Sreenath et al. (2011). Their biped, MABEL, was able to walk, run and step over obstacles by emulating a spring-mass model on each leg, through the leg's design and the hip's differential drive "(Organtzidis (2017)). Both of these bipeds are planar robots, relying on external lateral support to operate. The most noteworthy examples of untethered 3D walking belong to a series of robots whose morphology closely resembled the spring-mass model, ATRIAS (Rezazadeh et al. (2015) and MARLO (Buss et al. (2014)). All of these robots are based on abstract models with considerably reduced complexity compared to their actual body. They are close to the passive walkers of the past (McGeer (1990)), as they introduce some active control component to drive the body dynamics into desired stable regions. On the other end of the spectrum there are more detailed robots with HONDA's ASIMO (Sakagami et al. (2002)) being a representative example. "ASIMO is a biped that computes joint angle trajectories through inverse dynamics and tries to retain the Zero Moment Point (ZMP) (i.e centre of pressure on the foot) within the convex hull of the foot support to remain stable. Its control method is common in a large number of bipedal walkers " ((Organtzidis, 2017, p. 2-5)). ASIMO benefits from its segmented legs to achieve higher manoeuvrability than the rest of the mentioned bipeds, whereas its energy efficiency is compromised (ATRIAS expends less than one third the energy of ASIMO in comparable speeds, Rezazadeh et al. (2015)). Stability and energy efficiency were considered goals of higher priority, as they were more fundamental to both a walker's operation, as discussed in the **Introduction**. The promising performance of state-of-the-art legged robots whose control strategy revolved around controlling a version of the spring-mass system combined with the potential of such models to capture key features of human walking encouraged the extension of this basic model in 3D in the present work.

# Chapter 3

# Methods

In order to prove that the proposed 3D bipedal spring-mass model is able to walk stably, a sequence of computational methods were implemented. Initially, the analytical equations of motion for the model were derived for both the single support and double support phases. Consequently, different control laws were applied on the model and periodic patterns were sought in its phase space. Only patterns that exhibited asymptotic stability in the formal mathematical sense were kept and their robustness was finally evaluated by calculating the basin of attraction around their corresponding stable nodes in phase space.

## 3.1 Mathematical model

The model under consideration consisted of a point mass $m$ in place of the centre of mass and two massless legs with a linear spring constant $k$ and a resting length $l_r$. Its dynamics included 2 separate analytical expressions: one corresponding to single support, where one leg was in contact with the ground and another describing double support, where both legs were in contact. Through the Euler-Lagrange method, these equations were derived by first calculating the kinetic and potential energies of both phases:

$$T = \frac{1}{2}m(\dot{x}^2 + \dot{y}^2 + \dot{z}^2)$$

$$V = mgy + \frac{1}{2}k(l_r - \sqrt{x^2 + y^2 + z^2})^2 \quad \text{for single support}$$

$$V = mgy + \frac{1}{2}k(l_r - \sqrt{x^2 + y^2 + z^2})^2 + \frac{1}{2}k(l_r - \sqrt{(x-d)^2 + y^2 + (z-w)^2})^2 \quad \text{for double support}$$

The $x, y, z$ variables were the Cartesian coordinates of the mass $m$, whereas $d, w$ corresponded to the step length and width respectively and $g$ was the acceleration of gravity. The variables $\dot{x}, \dot{y}, \dot{z}$ described the components of the velocity vector along each axis. The Langragian function was then defined as $L = T - V$ and the equations of motion were derived by the equation :

$$\frac{d}{dt}\left(\frac{\partial L}{\partial \dot{q}}\right) - \frac{\partial L}{\partial q} = 0, \quad q = \begin{bmatrix} x \\ y \\ z \end{bmatrix} \in \mathbb{R}^3 \tag{3.1}$$

leading to the dynamics of the single support phase :

$$\ddot{x} = \frac{kx}{m}\left(\frac{l_r}{\sqrt{x^2+y^2+z^2}} - 1\right) \tag{3.2}$$

$$\ddot{y} = \frac{ky}{m}\left(\frac{l_r}{\sqrt{x^2+y^2+z^2}} - 1\right) - g \tag{3.3}$$

$$\ddot{z} = \frac{kz}{m}\left(\frac{l_r}{\sqrt{x^2+y^2+z^2}} - 1\right) \tag{3.4}$$

and that of double support :

$$\ddot{x} = \frac{kx}{m}\left(\frac{l_r}{\sqrt{x^2+y^2+z^2}} - 1\right) + \frac{k(x-d)}{m}\left(\frac{l_r}{\sqrt{(x-d)^2+y^2+(z-w)^2}} - 1\right) \tag{3.5}$$

$$\ddot{y} = \frac{ky}{m}\left(\frac{l_r}{\sqrt{x^2+y^2+z^2}} - 1\right) + \frac{ky}{m}\left(\frac{l_r}{\sqrt{(x-d)^2+y^2+(z-w)^2}} - 1\right) - g \tag{3.6}$$

$$\ddot{z} = \frac{kz}{m}\left(\frac{l_r}{\sqrt{x^2+y^2+z^2}} - 1\right) + \frac{k(z-w)}{m}\left(\frac{l_r}{\sqrt{(x-d)^2+y^2+(z-w)^2}} - 1\right) \tag{3.7}$$

Equations 3.2 to 3.7 were transformed into the dimensionless form in order to enhance the applicability of the results through different scales. This is a standard process in biomechanics, when systems are considered in a range of scales. The dimensionless variables were derived using only the design parameters of the system and gravity as :

$$\hat{x} = \frac{x}{l_r}, \quad \hat{y} = \frac{y}{l_r}, \quad \hat{z} = \frac{z}{l_r}, \quad \hat{k} = \frac{kl_r}{mg}, \quad \hat{d} = \frac{d}{l_r}, \quad \hat{w} = \frac{w}{l_r}, \quad \hat{v} = \frac{v}{\sqrt{gl_r}}, \quad \hat{E} = \frac{E}{mgl_r}$$

where $\hat{v}$ and $\hat{E}$ are the dimensionless velocity and total energy of the system. Consequently the dimensionless equations of motion were for single support

$$\ddot{\hat{x}} = \hat{k}\hat{x}\left(\frac{1}{\sqrt{\hat{x}^2+\hat{y}^2+\hat{z}^2}}-1\right) \tag{3.8}$$

$$\ddot{\hat{y}} = \hat{k}\hat{y}\left(\frac{1}{\sqrt{\hat{x}^2+\hat{y}^2+\hat{z}^2}}-1\right)-1 \tag{3.9}$$

$$\ddot{\hat{z}} = \hat{k}\hat{z}\left(\frac{1}{\sqrt{\hat{x}^2+\hat{y}^2+\hat{z}^2}}-1\right) \tag{3.10}$$

and for double support

$$\ddot{\hat{x}} = \hat{k}\hat{x}\left(\frac{1}{\sqrt{\hat{x}^2+\hat{y}^2+\hat{z}^2}}-1\right)+\hat{k}(\hat{x}-\hat{d})\left(\frac{1}{\sqrt{(\hat{x}-\hat{d})^2+\hat{y}^2+(\hat{z}-\hat{w})^2}}-1\right) \tag{3.11}$$

$$\ddot{\hat{y}} = \hat{k}\hat{y}\left(\frac{1}{\sqrt{\hat{x}^2+\hat{y}^2+\hat{z}^2}}-1\right)+\hat{k}\hat{y}\left(\frac{1}{\sqrt{(\hat{x}-\hat{d})^2+\hat{y}^2+(\hat{z}-\hat{w})^2}}-1\right)-1 \tag{3.12}$$

$$\ddot{\hat{z}} = \hat{k}\hat{z}\left(\frac{1}{\sqrt{\hat{x}^2+\hat{y}^2+\hat{z}^2}}-1\right)+\hat{k}(\hat{z}-\hat{w})\left(\frac{1}{\sqrt{(\hat{x}-\hat{d})^2+\hat{y}^2+(\hat{z}-\hat{w})^2}}-1\right) \tag{3.13}$$

The $(\hat{.})$ symbol was dropped for the remainder of the text as dimensionless variables were used exclusively. The dynamics equations 3.8 to 3.13 were two sets of continuous-time, second-order differential equations. There was no closed-form solution of either set and for numerical integration an initial position and velocity vectors were required, as each set had to be twice integrated. Thus, the state space was extended to $\begin{bmatrix}\dot{q} & q\end{bmatrix}^T \in \mathbb{R}^6$ and the following equations were added in both the single and the double support sets

$$\dot{x} = v_x \tag{3.14}$$

$$\dot{y} = v_y \tag{3.15}$$

$$\dot{z} = v_z \tag{3.16}$$

This way each set of 3 second-order differential equations was transformed into a set of 6 first-order differential equations that included both the position and velocity vectors. The final sets of 6 equations were integrated using the ode113 solver of the MATLAB(v.2016b) software package. The centre of mass trajectory during steady state walking was smooth and non-stiff, thus there was no need for more advanced solvers.

Additionally, ode113 performs better with stringent tolerances, as in the present case of relative and absolute tolerance of $10^{-12}$ and maximum integration step size equal to $10^{-3}$.

The centre of mass trajectory was governed by one of these sets at every moment in time, while a switch between sets was applied by one of two discrete events. The first event was leg touch-down and occurred when during single support, the free swinging leg came in contact with the ground, denoting the beginning of double support phase. The second event took place at the instance of lift-off when, during double support, the trailing leg reached its resting length $l_r$ and was lift off the ground, denoting the beginning of single support for the front leg. It was assumed that the legs were only able to contract and not extend during walking, for a more realistic representation of human walking. More formally, the switching conditions of the two events were expressed by the following equations

$$y_{TD} = \sin\theta, \quad \text{touch-down condition} \tag{3.17}$$

$$\sqrt{x_{LO}^2 + y_{LO}^2 + z_{LO}^2} = 1, \quad \text{lift-off condition} \tag{3.18}$$

Touch-down was additionally the instance, when control was applied to determine the position where the swing leg touched the ground. Figure 3.1 shows a draft of the saggital and horizontal planes during touch-down, along with the control variables $\theta = f(q, \dot{q})$ and $\beta = g(q, \dot{q})$. These two angles corresponded to frontal and lateral leg angles respectively, as discussed in the **Literature Review** chapter (Figure 2.1). The functions $f, g : \mathbb{R}^6 \to \mathbb{R}$ represented different analytical expressions according to the applied leg placement strategy. Several strategies were tested that fell into the definition of simple control, as they only depended on centre of mass position and/or velocity. They are presented in more detail in the following section. During touch-down the equation

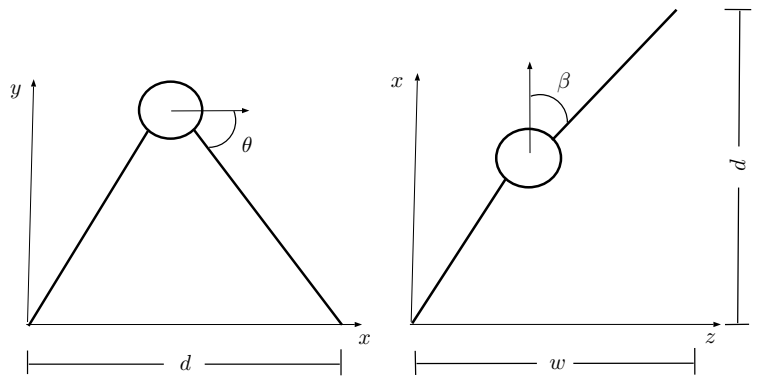


(a) Saggital plane (b) Horizontal plane

Figure 3.1: Moment of touch-down with control variables $\theta$ and $\beta$

$\sqrt{(x-d)^2+y^2+(z-w)^2}=1$ also held, implying that the swing leg touched the ground at its natural length, which was $\frac{l_r}{l_r}=1$ in the non-dimensional case. The step length and width were calculated at the touch-down event by the equations

$$d = x + \cos\theta\cos\beta \tag{3.19}$$

$$w = z + \cos\theta\sin\beta \tag{3.20}$$

Figure 3.2 included both single and double support phases split by the touch-down and lift-off events for one full stride (i.e one left and one right step of the model). Transver-

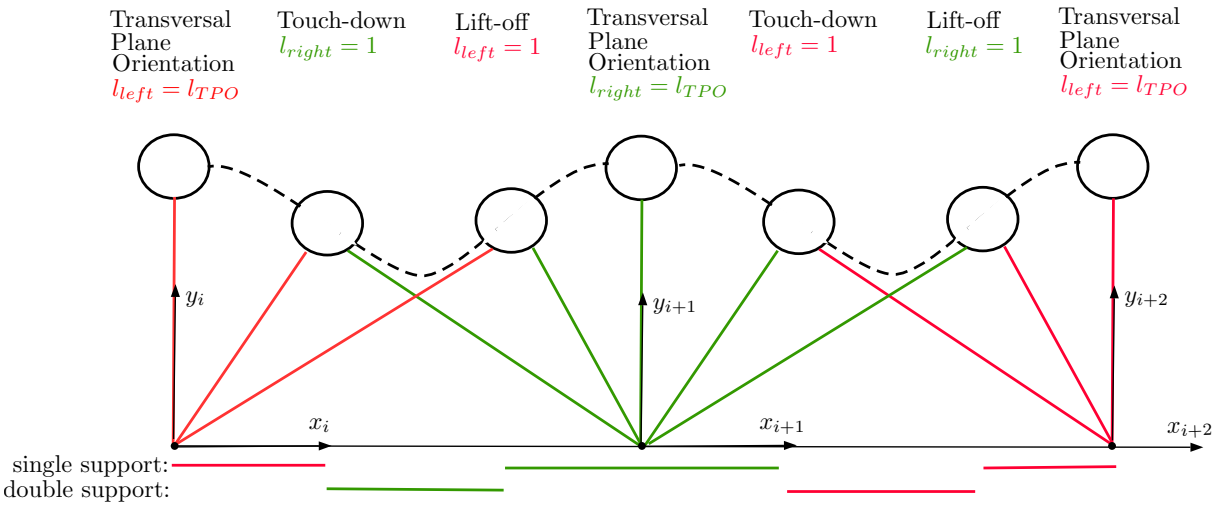


Figure 3.2: Saggital plane view of one full stride

sal plane orientation, as depicted in Figure 3.2, described the time instance when the $x$ component of centre of mass position was equal to zero. In other words, during this moment, the leg and by extension the centre of mass belonged to a plane that was perpendicular to the walking direction. The equivalent of this orientation has been widely used in 2D walking (Geyer et al. (2006), Rummel et al. (2010), Vejdani et al. (2015)) as the initial state of a step, since it eliminated one component of the state space vector ($x = 0$) and reduced the dimensionality of the phase space for stable patterns. The same idea was implemented in the current analysis, although instead of having the leg oriented vertical to the ground, it was orientated along the transversal plane, as shown in Figure 3.3. Depending on the orientation of the velocity vector $\dot{q}_0$, with $v_0 = \|\dot{q}_0\|$, at the transversal plane orientation instance, symmetric and asymmetric walking patterns can emerge. This was shown for the 2D case in Rummel et al. (2010). During symmetric walking, the ground reaction forces on the legs follow an identical profile and can be mirrored around the transversal plane orientation moment during each left or right step. In contrast, asymmetric walking does not include any point of symmetry along a single step and the force profiles may not match between left and right steps. Figure

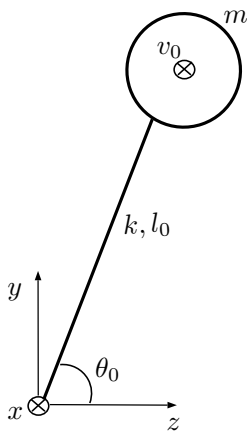


Figure 3.3: Transversal plane orientation

3.4 includes an example of symmetric and one of asymmetric walking, as found by the present analysis. Non-dimensional forces in the figures were expressed as ratios of body weight.

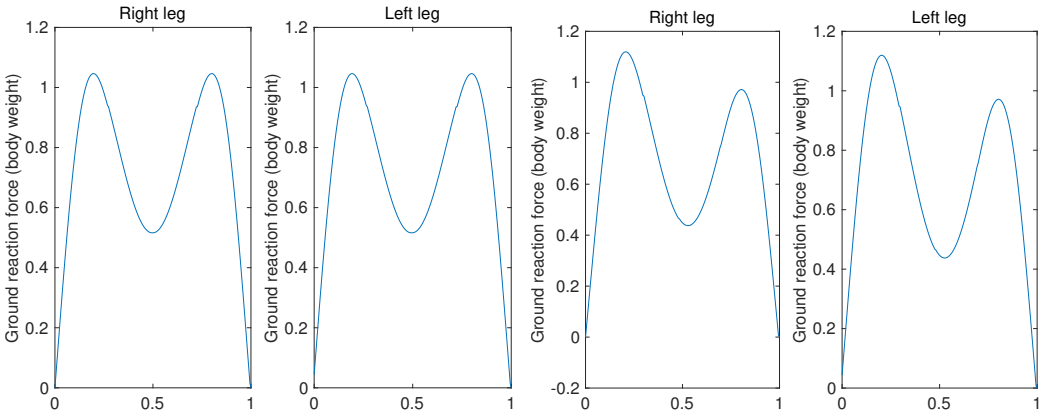


(a) Symmetric walking (b) Asymmetric walking

Figure 3.4: Qualitative examples of the 2 pattern types

The point of symmetry coincided with the transversal plane orientation for symmetric walking at 0.5 of either left or right steps. Since no work was previously done in identifying and classifying 3D walking patterns, the focus of this project was on symmetric walking. The identical profiles of the applied force on both legs during symmetric walking could simplify the structural design and material choices of a legged robot. Another valuable point is that symmetry can be expressed as an analytical expression, reducing the size of the phase space. The phase space vector has $4$ dimensions, derived from the state space vector, the initial event of transversal plane orientation and the conservative nature of the model. An extensive investigation of the phase space for the determination of stable nodes and calculation of their basins of attraction would have

been unrealistic in terms of the project's duration. Thus, the analytical equations that govern symmetric walking were used to more efficiently manage time in addition to the benefit of having the same force profile applied on each leg during steady state walking. At the transversal plane orientation of symmetric patterns, the $y, z$ coordinates were at the maximum of their oscillation with their components of velocity equal to zero. This implied that there was no vertical or lateral momentum acting on the leg and thus the sum of centrifugal, spring forces and the component of gravitational pull acting along the leg axis (radial direction) was equal to zero.

$$\Sigma F_{radial} = 0 \Rightarrow k(1 - \sqrt{y_0^2 + z_0^2}) + \frac{v_0^2}{\sqrt{y_0^2 + z_0^2}} - \sin\theta_0 = 0 \tag{3.21}$$

$$\Rightarrow \sqrt{y_0^2 + z_0^2} = l_0 = \frac{k + \sin\theta_0 \pm \sqrt{k^2 + 2k\sin\theta_0 + \sin^2\theta_0 - 4k\sin\theta_0 + 4kv_0^2}}{2k} \tag{3.22}$$

Additionally, the system was conservative, operating at a predetermined energy level

$$E = T + V = \frac{1}{2}v^2 + \frac{1}{2}k(1 - \sqrt{x^2 + y^2 + z^2})^2 + y = \text{constant} \tag{3.23}$$

$$\text{this led to} \quad v_0 = \sqrt{2E - k(1 - \sqrt{y_0^2 + z_0^2})^2 - 2y_0} \quad \text{in the initial state} \tag{3.24}$$

In fact, at every instance the velocity magnitude was exclusively a function of $q$. Thus, 2 spherical angles, the polar angle $\phi$ and azimuthal angle $\psi$ were sufficient to describe the velocity vector. Equations 3.22 and 3.24 form a 2x2 system of nonlinear equations, the solution of which yielded the initial velocity magnitude $v_0$ and initial leg length $l_0$ for symmetric walking, given the initial leg angle on the transversal plane $\theta_0 \in [84^o, 89^o] \rightarrow [1.466, 1.553]$ radians (Figure 3.3). The range of $\theta_0$ was chosen based on experimental observations of human walking, where the maximum deflection of the centre of mass was approximately $5^o$ (Kuo (1999)). The full state vector $\begin{bmatrix}\dot{q}_0 & q_0\end{bmatrix}^T$ was then directly calculated in order to sequentially integrate the equations of motion 3.8 to 3.13

$$\dot{q}_0 = \begin{bmatrix}\dot{x}_0 \\ \dot{y}_0 \\ \dot{z}_0\end{bmatrix} = \begin{bmatrix}v_0\cos\phi_0\cos\psi_0 \\ \sin\phi_0 \\ v_0\cos\phi_0\sin\psi_0\end{bmatrix} = \begin{bmatrix}v_0 \\ 0 \\ 0\end{bmatrix} \tag{3.25}$$

$$q_0 = \begin{bmatrix}x_0 \\ y_0 \\ z_0\end{bmatrix} = \begin{bmatrix}0 \\ l_0\sin\theta_0 \\ l_0\cos\theta_0\end{bmatrix} \tag{3.26}$$

Concluding, the phase space vector of independent variables that described a walking

pattern was

$$\begin{bmatrix} y_0 & z_0 & \phi_0 & \psi_0 \end{bmatrix}^T \in \mathbb{R}^4 \tag{3.27}$$

by setting the transversal plane orientation as initial state. The following sections introduce the control laws that were tested for stable walking and the methods employed in the search for stable solutions.

## 3.2 Leg placement control

After formulating the model equations, the control law employed to place the swing leg to a specific location in contact with the ground was determined. All laws considered were functions of some subspace of the full state space $\begin{bmatrix} \dot{q} & q \end{bmatrix}^T$. They can be considered simple, as they only require information about the position and/or velocity of the centre of mass at the touch-down event ( $(.)_{TD}$ index) in order to stabilise the walking movement. The list of all considered strategies for frontal leg placement is

$$\theta = \text{constant}, \quad \theta \in [0.85, 1.32] \text{ radians} \tag{3.28}$$

$$\theta = \tan^{-1}\left(\frac{v_{y,TD}}{\sqrt{v_{x,TD}^2 + v_{z,TD}^2}}\right) + \theta_c, \quad \theta_c \in [0, 1] \text{ radians} \tag{3.29}$$

$$\theta = \tan^{-1}\left(\frac{v_{y,TD}}{\sqrt{v_{x,TD}^2 + v_{z,TD}^2}}\right)(1 - r_\theta) + r_\theta \frac{\pi}{2}, \quad r_\theta \in [0, 0.9] \tag{3.30}$$

whereas the strategies utilised for lateral leg placement are

$$\beta = \text{constant}, \quad \beta \in [0.04, 0.9] \text{ radians} \tag{3.31}$$

$$\beta = \tan^{-1}\left(\frac{v_{z,TD}}{v_{x,TD}}\right) + \beta_c, \quad \beta_c \in [0.03, 0.12] \text{ radians} \tag{3.32}$$

$$w = z_{TD} + \frac{v_{z,TD}}{\sqrt{k}} + z_c \rightarrow \beta = \sin^{-1}\left(\frac{w - z_{TD}}{\cos\theta}\right), \quad z_c \in [0.01, 0.06] \tag{3.33}$$

All possible combinations resulted in 9 strategies for leg placement by adjusting $\theta, \beta$ angles. Functions 3.28 to 3.32 were first proposed in Peuker et al. (2012), where they were applied on the 3D spring-mass running model, that included a single support and an aerial, ballistic flight, phase. They described two different ways to adjust the lateral angle $\beta$, either from a fixed external reference frame 3.31 or egocentrically, based on

the velocity vector 3.32, and three different options for the frontal angle $\theta$: fixed external reference frame 3.28 or egocentrically, either at a fixed angle from the velocity vector 3.29 or as a ratio of the total angle between velocity and gravity vectors 3.30. For clarity, they are depicted in Figure 3.5, as presented in the original work. With an exception for the pairs 3.28-3.31 and 3.30-3.31, the rest have resulted in stable running and thus encouraged their extension to walking.

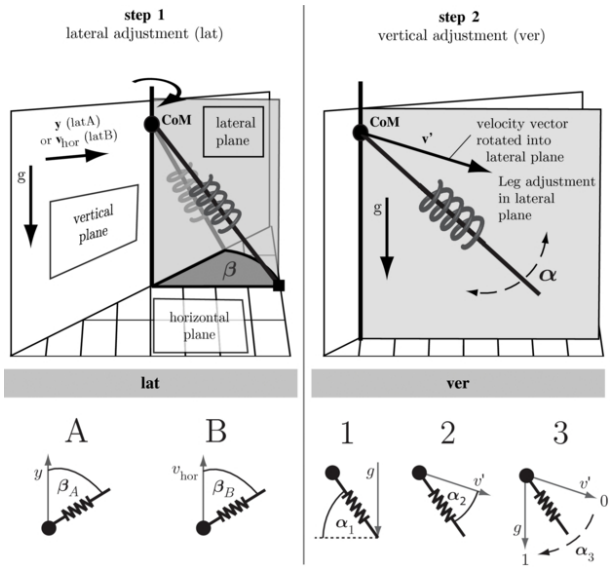


Figure 3.5: Leg placement strategies taken from Peuker et al. (2012)

Function 3.33 was an analytical expression of the observed behaviour in the walking experiments of Hof et al. (2007). The term $\sqrt{k}$ corresponded to the natural frequency of the spring leg for the non-dimensional case and differed from the original value of $1$, as the referenced work used an inverted pendulum model with stiff legs to describe the experimental results. This observed behaviour of the lateral leg angle was combined with the three options for $\theta$ adjustment for the potential abstraction of human walking dynamics by the current model.

Additionally, a strategy with constant step length and width was the $10^{th}$ option evaluated for stability. The hypothesis behind this last strategy was to investigate whether the system could remain stable by taking steps of constant width and length. In this case the touch-down condition changed to $\sqrt{(x_{TD}-d)^2+y_{TD}^2+(z_{TD}-w)^2}=1$, which was valid as discussed in the previous section. Thus the touch-down position of the centre of mass was calculated through integration and the strategy was implemented by the following equations

$$\theta = \tan^{-1}\left(\frac{y_{TD}}{d-x_{TD}}\right), \quad d \in [0.3, 0.9] \tag{3.34}$$

$$\beta = \tan^{-1}\left(\frac{w - z_{TD}}{d - x_{TD}}\right), \quad w \in [0.03, 0.3] \tag{3.35}$$

The noted minima and maxima of the independent variables in equations 3.28 to 3.35 were tuned after executing simulations on larger, coarsely discretised ranges and focusing on physically preferable leg placement parameters for the final search in a finer grid. There were objective physical limitations, as the leg can not be placed behind the centre of mass, which resulted in $\theta, \beta \in [0, \frac{\pi}{2}]$. Additionally, angle values (or distances in the last strategy) that would result in very wide or short steps were excluded.

## 3.3 Stability analysis

It has been shown that bipedal walking with spring legs can be modelled as a hybrid dynamical system (Geyer et al. (2006)). The present work extended the previously proposed 2D walking model in 3D, producing a model that comprised of two continuous-time sets of equations 3.8 to 3.13 combined with 3.14 to 3.16, split between them by the two discrete events of touch-down 3.17 and lift-off 3.18. The transversal plane orientation was chosen as the initial state, therefore a third event was introduced to mark this state. A stride was also assumed to begin on the left leg. Periodic walking corresponded to limit cycles of this hybrid dynamical system, where the phase space vector 3.27 took identical values after one stride ($s_i = s_{i+2}$ in Figure 3.2). Using the notion of a Poincare map $P : \mathbb{R}^4 \to \mathbb{R}^4$ (Strogatz (2015)), a pattern was identified as periodic when

$$s_i = P(s_i) \Rightarrow s_i - P(s_i) = 0 = H(s_i) \tag{3.36}$$

for any stride starting on the $i_{th}$ step. Here it was assumed that all strides began on the left leg. Consequently, the function $P$ maps the state vector $s$ from one instance of transversal plane orientation of left leg to the next instance of the same event. There was no analytical expression for this map and it was evaluated after integrating the single and double support phases that occur within a stride. $H(s_i)$ represented a set of 4 equations, the solution of which was determined by applying a custom-made Newton-Raphson root-finding algorithm. The Newton-Raphson method ensures quadratic convergence to the closest root, given that the initial state of the algorithm, $s_0$ in this case, is close enough to the root. Since symmetric walking had higher priority as discussed above, the solution of the set of 3.22 and 3.24 ensured a good guess for the initial $y_0, z_0$ components of $s_0$. The other two ($\phi_0, \psi_0$) were set equal to zero, as the velocity at the

transversal plane orientation was oriented forward with no component along the $y, z$ axes for symmetric walking (equation 3.25). Therefore, after choosing a leg stiffness $k$ and an energy level $E$, only the initial leg angle $\theta_0$ was left as an independent variable. By exploiting the analytical expressions that described symmetric walking, the search space had been reduced considerably in size. It is noted additionally that if the model indicated falling ($y_{LO} < y_{TD}$) after double support, started moving backwards ($v_x < 0$) or extended its legs past the natural length ($\sqrt{x^2 + y^2 + z^2} > 1$) at any point during walking, then simulation was aborted and the algorithm moved on to the next value of $\theta_0$ and a new initial guess.

There exist more mathematically rigorous approaches applied on similar yet simpler problems. Merker et al. (2015) identified all the regions of stable walking for the 2D model by treating it as a boundary value problem. However this implementation was not straightforward, as the system was transformed from a hybrid dynamical system to a large set of nonlinear algebraic equations that required specialised software packages to be solved efficiently and accurately. Altendorfer et al. (2004) proposed a more advanced mathematical technique for the stability analysis of the 3D spring-mass running model. The Poincare map $P$ was factorised into two components, each one corresponding to either single support or flight phase. This was possible by exploiting the analytical nature of the flight phase, which was represented as a ballistic flight. The authors formulated sufficient conditions for instability and necessary ones for stability based on the flight phase factor of the Poincare map, an approach that can not be directly applied to walking, which consists of two non-integrable phases (single and double support). Possibly, appropriate simplifying assumptions could be made that would result in a similar factorisation of the current model, but advanced mathematical topics were beyond the scope of this work. Approaching the stability analysis problem as an initial value problem, solved by the Newton-Raphson method, was considered a fair negotiation of the trade-off between mathematical rigour and ease of implementation. It is a sufficiently accurate method, particularly as the current work was focused on identifying symmetric patterns and not covering all plausible values along the 4 dimensions of $s$, a task that would have been computationally more expensive and thus unrealistic in terms of the project's duration.

Roots of $H(s)$ corresponded to limit cycles of the 3D bipedal model that carried no information about how stable the cycle was. The stability of each solution was assessed

by calculating the eigenvalues $\lambda_j, j \in \{1, 2, 3, 4\}$ of the Jacobian of the Poincare map $P$

$$J = \frac{dP}{ds} = \begin{bmatrix} \frac{\partial P_y}{\partial y} & \frac{\partial P_y}{\partial z} & \frac{\partial P_y}{\partial \phi} & \frac{\partial P_y}{\partial \psi} \\ \frac{\partial P_z}{\partial y} & \frac{\partial P_z}{\partial z} & \frac{\partial P_z}{\partial \phi} & \frac{\partial P_z}{\partial \psi} \\ \frac{\partial P_\phi}{\partial y} & \frac{\partial P_\phi}{\partial z} & \frac{\partial P_\phi}{\partial \phi} & \frac{\partial P_\phi}{\partial \psi} \\ \frac{\partial P_\psi}{\partial y} & \frac{\partial P_\psi}{\partial z} & \frac{\partial P_\psi}{\partial \phi} & \frac{\partial P_\psi}{\partial \psi} \end{bmatrix} \tag{3.37}$$

where $P_y, P_z, P_\phi, P_\psi$ corresponded to the 4 components of the Poincare map and the phase space vector. The Jacobian $J$ was also needed during the Newton-Raphson algorithm for focusing along the direction of a root and was approximated by finite forward differences by introducing infinitesimal perturbations to the state vector $s$ during each iteration. It has been mathematically proven for the eigenvalues of 3.37, termed *Floquet multipliers*, that if $max(|\lambda|) < 1$, where $\lambda \in \mathbb{C}^4$ was the vector of all eigenvalues, then the system is asymptotically stable (Strogatz (2015)). The case of $max(|\lambda|) = 1$ corresponded to neutral stability, whereas if a multiplier was greater than 1, the system is unstable. The perturbation size was set to $10^{-8}$ and a periodic pattern was identified if $\|s_{k+1} - s_k\| < 10^{-6}$ for two consecutive iterations of Newton-Raphson.

Solutions of 3.36 that additionally proved to be asymptotically stable corresponded to stable nodes, $s_{st}$, in phase space. When applied on the model as initial conditions, they resulted in the limit cycles of the system. The stability of the limit cycles was evaluated by calculating the size of the basin of attraction around them. This was a representative metric of robustness commonly employed in dynamical systems theory (Strogatz (2015)) and more specifically in locomotion models (Peuker et al. (2012), Rummel et al. (2010)). Mathematical methods that calculate the boundary of the basin of attraction of a stable node require the determination of additional points in phase space, termed saddle nodes. Saddle nodes are characterised by one eigenvalue greater than and the rest less than 1. By computing backwards in time starting from the saddle node, the set of all points that lead to it are calculated. It was shown in Parker and Chua (1989) that these points also enclose the original stable node. However, it was not guaranteed that saddle nodes could be found around the stable node and even when they were found, the necessary computational process was a complex one to implement. Alternatively, a more intuitive approach was followed that exploited the definition of the basin of attraction. Perturbed phase space vectors $s_{pert}$ were used as initial conditions for the model and a maximum number of 50 walking steps was performed. If the model did not fall during the 50 steps and the condition $\|s_{pert,f} - s_{st}\| < 10^{-2}$ held, where $s_{pert,f}$ was the final phase space vector in the perturbed case, it was assumed that the point $s_{pert}$ belonged to the basin of attraction of $s_{st}$. The number of 50 steps was chosen to be sufficiently yet not unrealistically large, by arguing that any system that managed

to remain stable for 50 steps under some perturbation and while relying on its passive body dynamics had sufficient time to apply some other, possibly higher-level, form of control to reach a desired state.

# Chapter 4

# Results

The sequential process that was presented in the previous chapter was applied for the 10 proposed leg strategies. A search for periodic solutions among the considered ranges of parameters of each strategy (equations 3.28 to 3.32) was the first step. Consequently, periodic solutions were assessed for stability in terms of the magnitude of the *Floquet multipliers* and those that proved to be stable were finally perturbed in order to calculate the borders of their basins of attractions. The results from every step of this analysis are presented below.

Initially a leg stiffness value of $k = 17.8389$ and an energy level $E = 1.0398$ were chosen as the model parameters. In the 2D case this set of values has led to a robust solution, as shown in Rummel et al. (2010), and matched sufficiently well experimental walking data in Geyer et al. (2006). Thus, it was a promising candidate for robust walking in 3D. Among the 10 proposed leg strategies that were introduced in the **Leg placement control** section of the previous chapter, two of them resulted in stable walking. The pair of equations 3.28 and 3.32, termed *beta* strategy in the present work, led to 29 symmetric walking patterns. As a reminder, this strategy places the leg at a fixed frontal angle $\theta$ and at a lateral angle $\beta$ that is at fixed angle to the side of the velocity vector at touch-down. The second successful strategy, termed *ratio-beta*, involved the same equation 3.32 for $\beta$ calculation, whereas $\theta$ was the sum of a ratio of the total angle between the velocity and gravity vectors and the polar angle of velocity at touch-down (equation 3.30). *Ratio-beta* strategy resulted in 19 patterns, only one of which was symmetric. The rest of the identified patterns were close enough to symmetric, as the Newton-Raphson algorithm managed to converge to them with an initial guess for symmetric walking. Two representative examples from this strategy were depicted in Figure 3.4. Even though asymmetries were evident in the system's dynamics, step

length, width and time were equal (differences $< 10^{-12}$) between left and right leg in every pattern of both strategies.

The condition $max|\lambda| = 1$ held for all the identified patterns for both control strategies. This result was expected, since $\beta$ adjustment in both strategies was relative to the velocity vector. It was thus based on an egocentric frame of reference, rather than an external one. Maus and Seyfarth (2014) has shown that the *beta* strategy was able to predict the circular gait that disoriented or blind people exhibit, as they do not have an external reference. Mathematically this translates to neutral stability along the $\psi$ direction of the phase vector $s$ 3.27, resulting in a change of walking direction under an arbitrary perturbation of this component. Asymptotic stability was however achieved along the other 3 directions in state space. The following results made apparent the fact that the model was able to walk robustly, even under perturbations and changes to its walking direction.

Since there was no pattern that exhibited asymptotic stability along the azimuthal velocity angle $\psi$, the analysis of robustness was performed on the other three dimensions of $s$. Initially, a grid of $y_{pert} \in [0.9, 1]$ and $z_{pert} \in [0, min(0.1, \sqrt{1-y^2})]$ values was formed as the perturbed initial vector $s_{pert}$ along with $\phi_{pert}$ and $\psi_{pert}$, which were kept equal to the values of the respective stable node. The original condition for a perturbed state to lie within the basin of attraction of a stable node ($\|s_{pert,f} - s_{st}\| < 10^{-2}$) was updated to include the Euclidean norm along the $y, z, \phi$ dimensions, excluding $\psi$.

The upper bound of the considered perturbations corresponded to the resting leg length $\sqrt{y_{pert}^2 + z_{pert}^2} = 1$, whereas the lower bound was tuned to ensure that the lower feasible height was included for every pattern, since the condition $y_{pert} > y_{TD}$ had to hold. In the case of *beta* strategy, the touch-down height $y_{TD} = \sin\theta$ was predetermined, as $\theta =$ constant. However, $y_{TD}$ in the *ratio-beta* pattern depended on the velocity vector at touch-down, thus integration of the single support equations was necessary before its value was known. Tuning through iterative walking simulations resulted in the above lower $y$ bound. The calculated basins of attractions for each pattern are presented in Figure 4.1 for the *beta* strategy and in Figure 4.2 for the *ratio-beta* one The positions of the stable nodes and the areas of the boundary polygons of the basins of attractions are included for clarity.

Additional analysis was conducted for $\phi_{pert} \in [-\frac{\pi}{2}, \frac{\pi}{2}]$. The resulted stable regions for perturbations within this range are included in Table 4.1. Combined perturbations of $y, z$ and $\phi$ were not tested. Initial simulations indicated forbidding computational times for the duration of this project. Moreover, it was more meaningful to separate spatial

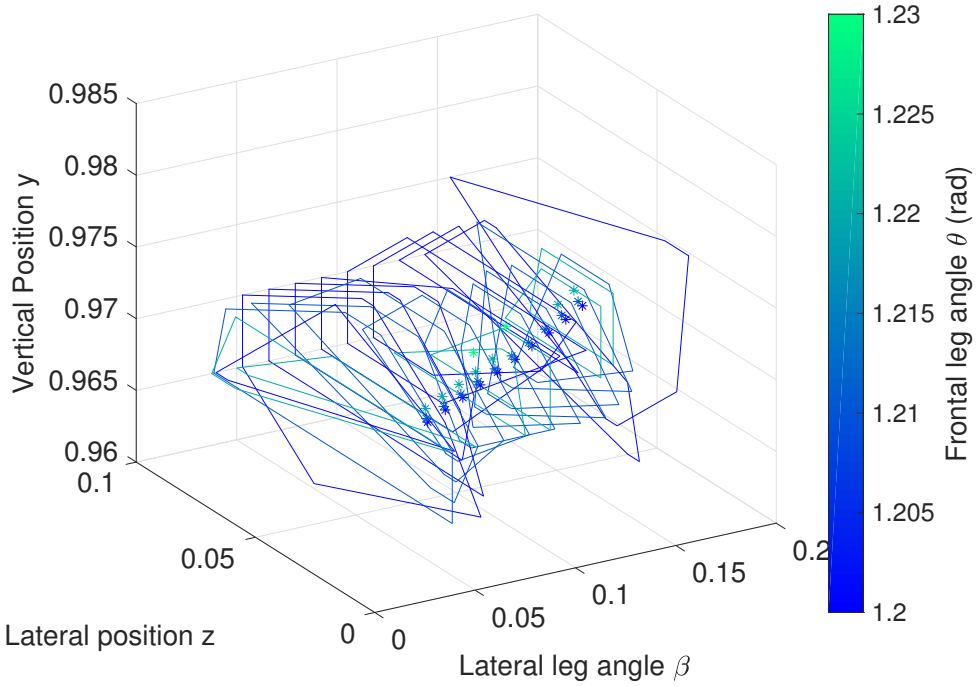


(a) Basin of attraction for all found patterns

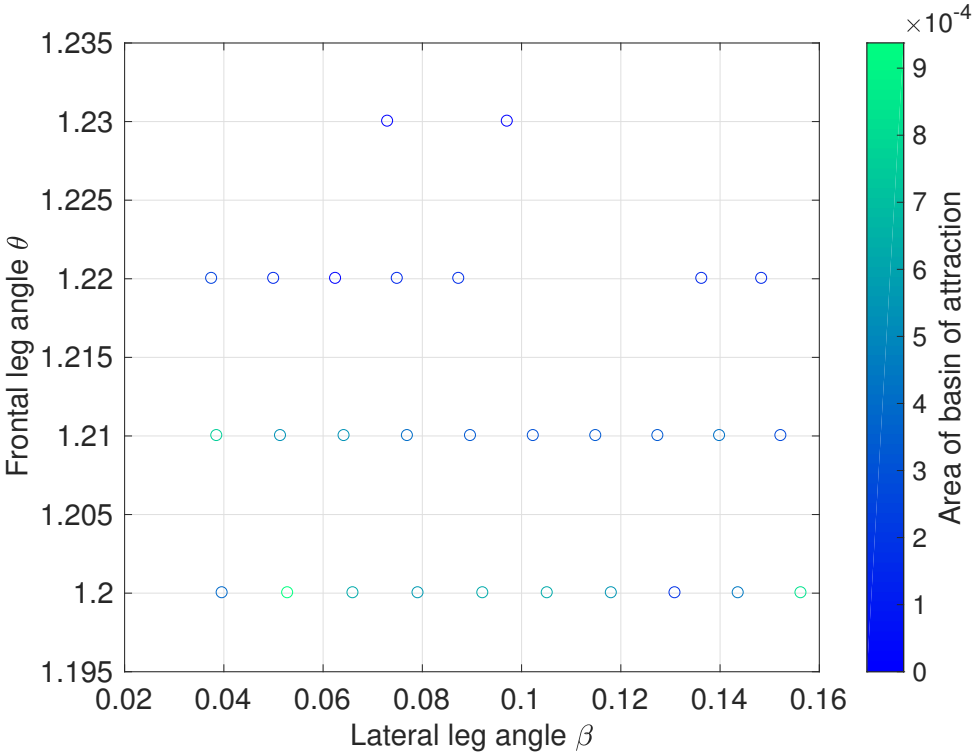


(b) Area of each basin as a function of $\theta$ and $\beta$

Figure 4.1: *Beta* strategy

perturbations along $y, z$ and velocity perturbations, modelled by changes of the polar angle $\phi$. The former simulated perturbed foot positions, for example variations in the ground height (as applied for the 3D running model in Wu and Geyer (2013)) or in lateral

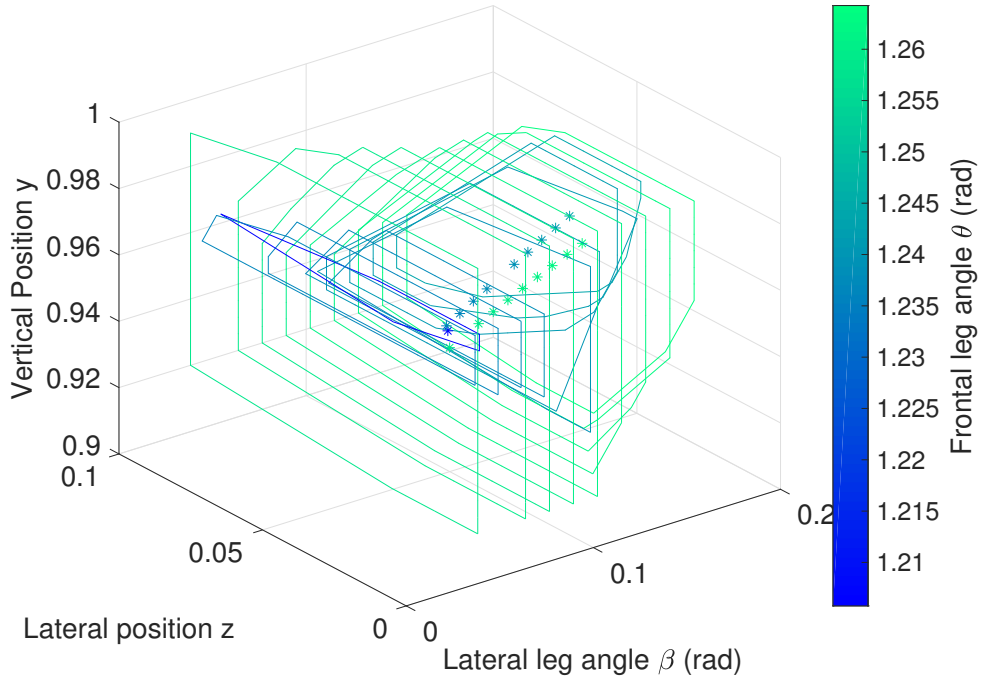


(a) Basin of attraction for all found patterns

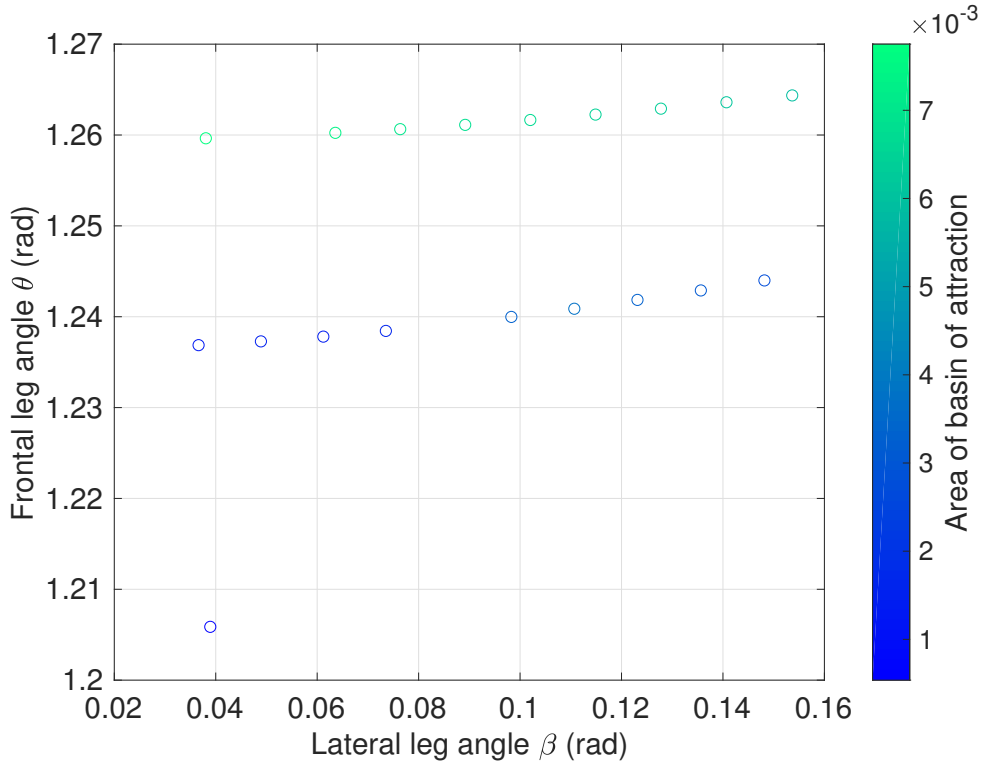


(b) Area of each basin as a function of $\theta$ and $\beta$

Figure 4.2: *Ratio-beta* strategy

foot position. The latter was used to model the effect of abrupt forces, whose application time was short enough to assume that velocity was perturbed whereas centre of mass position remained constant (Hof et al. (2010), Oddsson et al. (2004) for experimental

applications on human walking).

A comparison with a finer grid was performed for 2 patterns, one from each strategy, with the most similar step length ($\Delta d = 2.2 \cdot 10^{-3}$), width ($\Delta w = 28.6 \cdot 10^{-3}$) and time ($\Delta t_{step} = 0.9 \cdot 10^{-3}$) values. Figure 4.3 includes the shaded basins of attraction for both patterns. Perturbations were performed along the $y$ and $z$ coordinates, while $\phi$ and $\psi$ remained equal to the steady state values of the corresponding limit cycle.

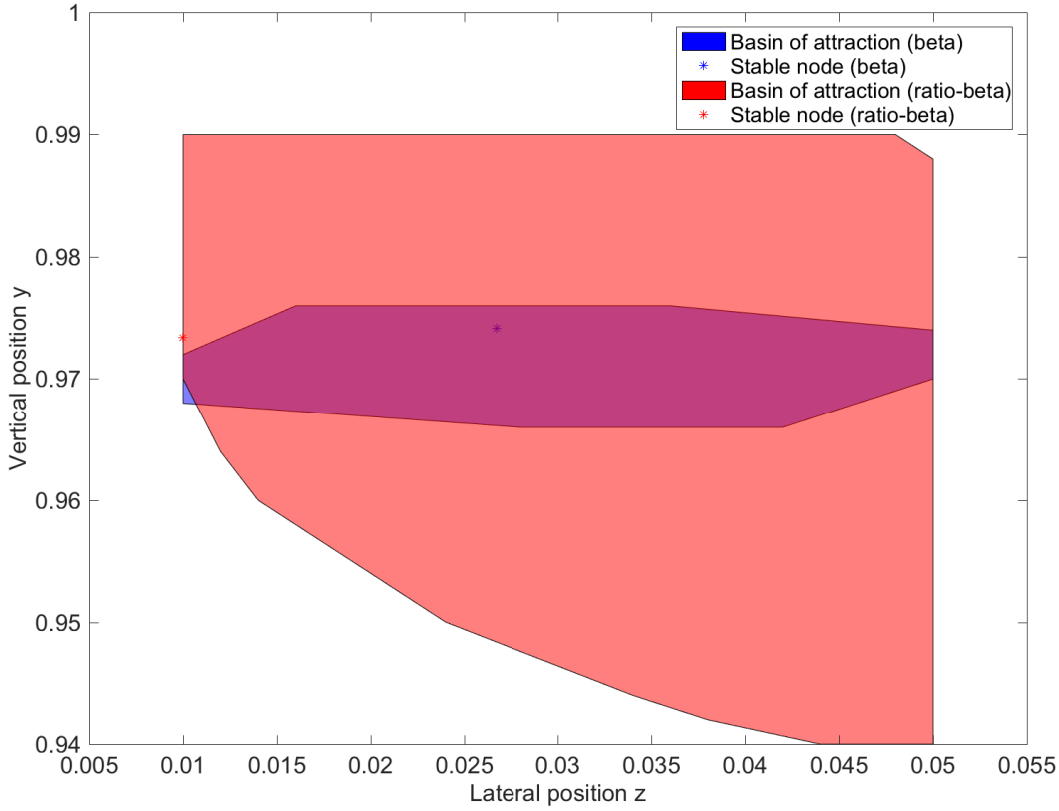


Figure 4.3: Basins of attraction of 2 patterns from each strategy with most similar gait parameters

The investigation was extended into 2 more values of leg stiffness for the *ratio-beta* strategy, as it had exhibited superior robustness compared to the *beta* strategy. The energy level was kept constant, while the stiffness values under consideration were $k = 15$ and $k = 20$. The value of $15$ had led to the most robust solution for the 2D walking model in Rummel et al. (2010). The stable patterns of the system with altered stiffness values were evaluated within the same perturbation ranges as the original system. Figures 4.4 and 4.5 present the resulted basins of attraction.

The results of the gait parameters of interest (step length, width, time and forward ve-

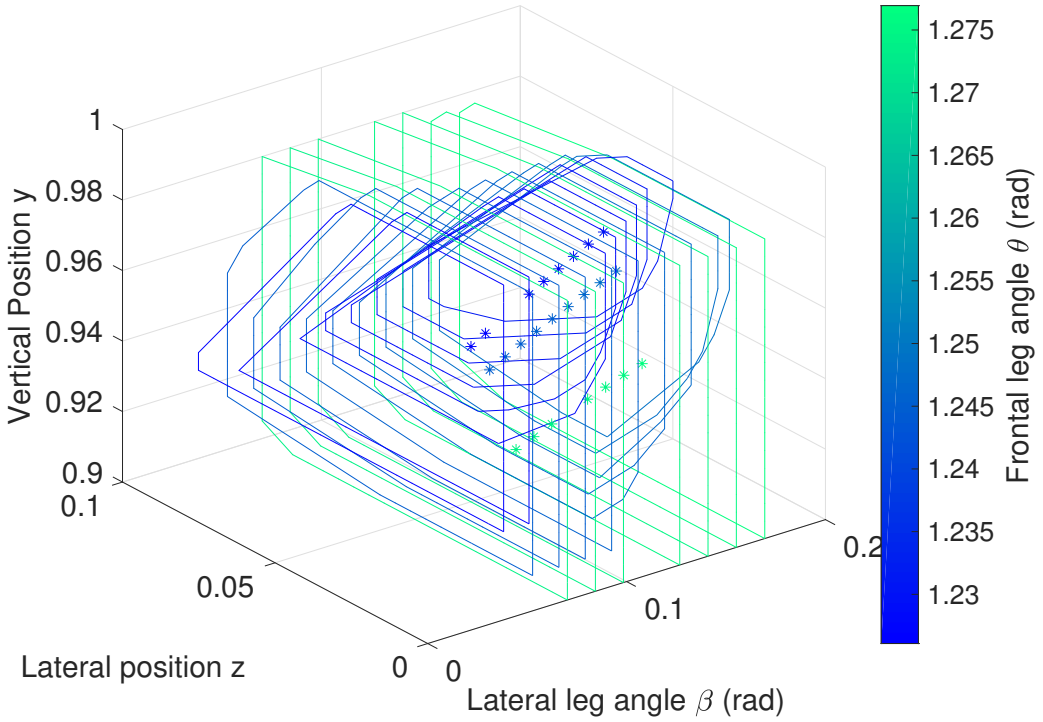


(a) Basin of attraction for all found patterns

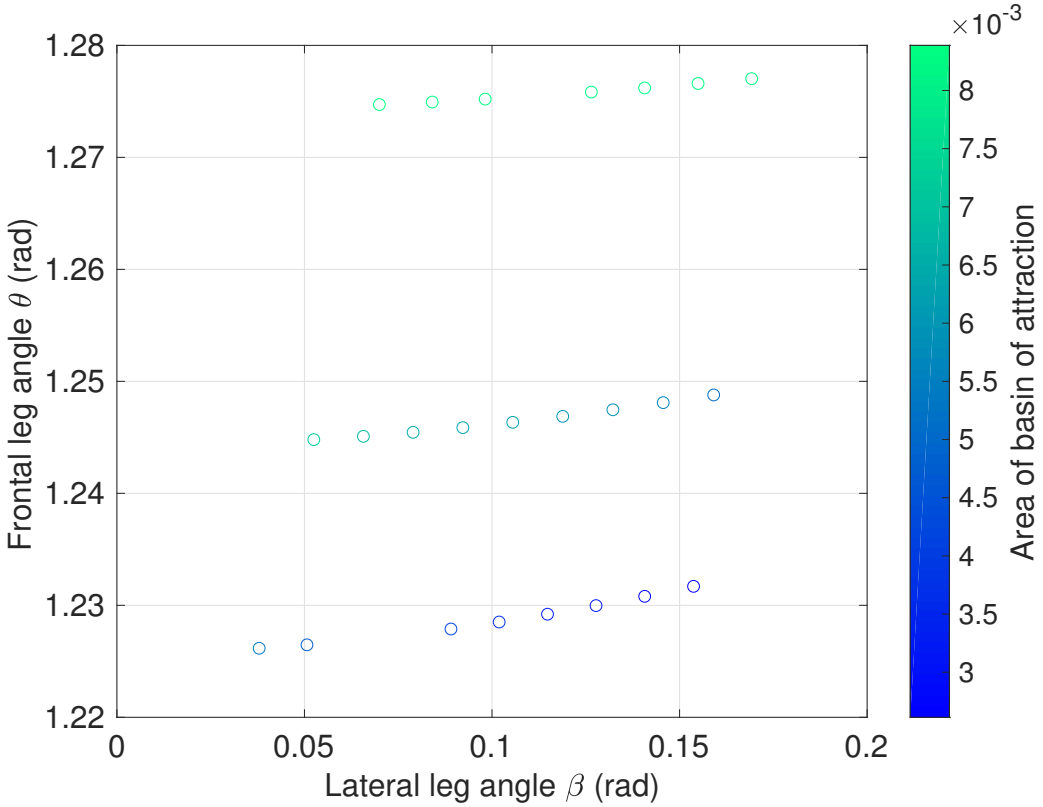


(b) Area of each basin as a function of $\theta$ and $\beta$

Figure 4.4: *Ratio-beta* strategy for $k = 15$

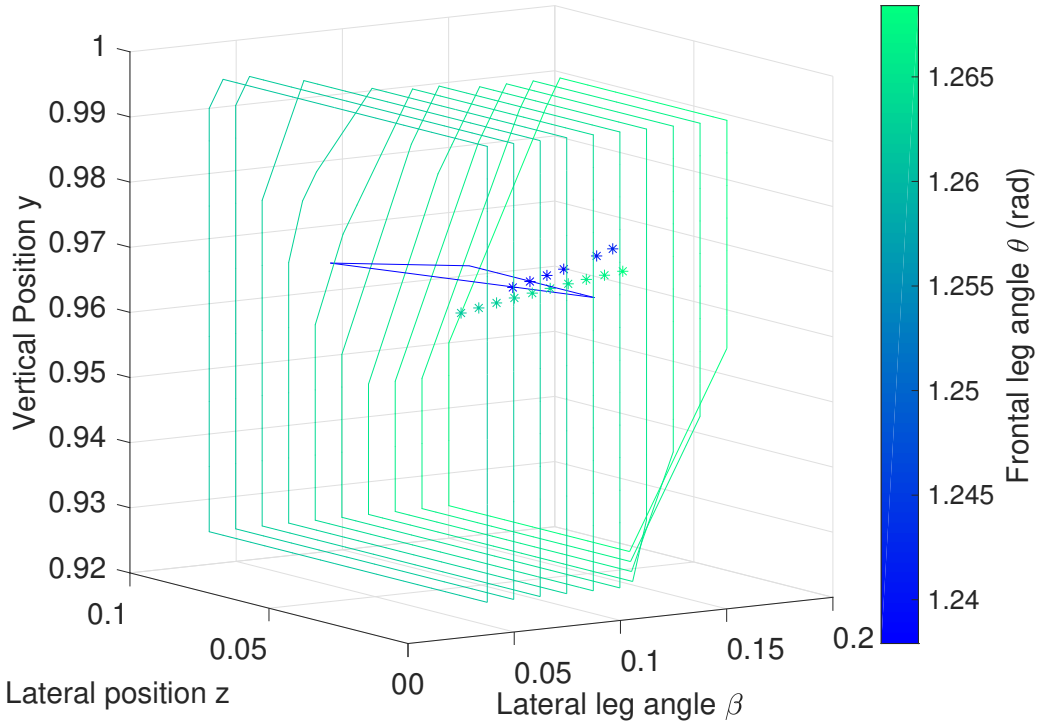


(a) Basin of attraction for all found patterns

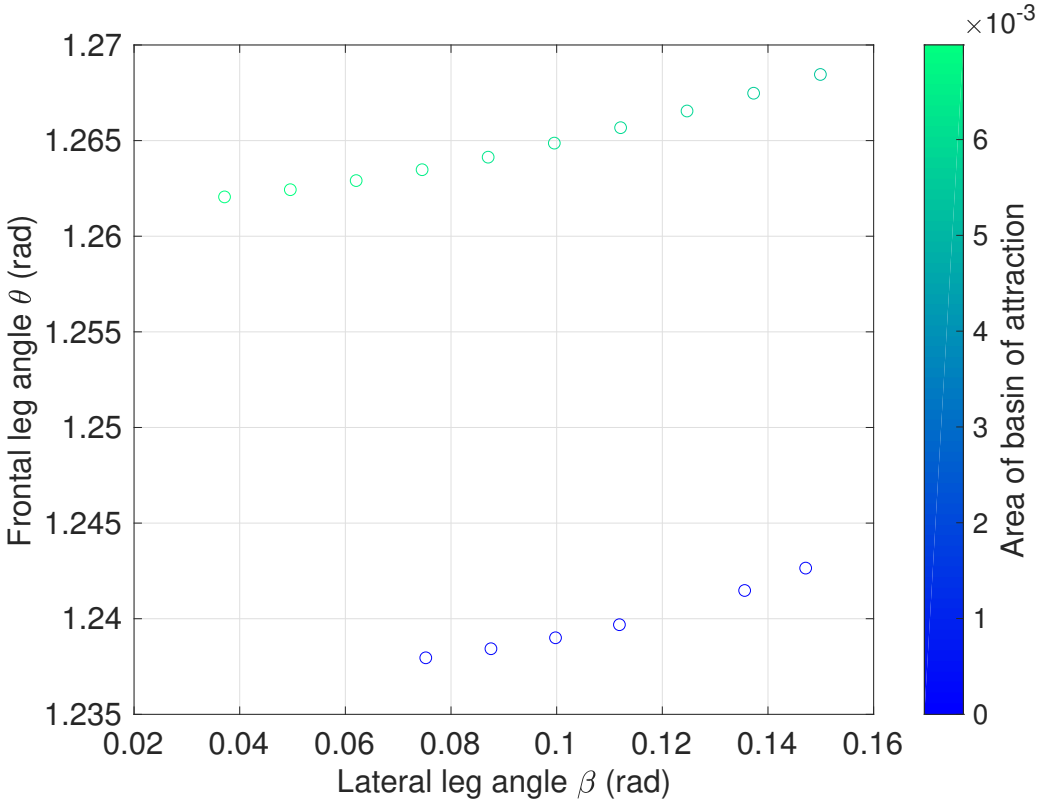


(b) Area of each basin as a function of $\theta$ and $\beta$

Figure 4.5: *Ratio-beta* strategy for $k = 20$

locity) and the robustness metrics (perturbations along $y, z$ and $\phi$ that converged to the stable node after 50 steps) are summarized in Table 4.1. Mean values and standard deviations of these values were calculated among the stable patterns of *beta* and *ratio-beta* strategies for the initial leg stiffness and for $k = 15$ and $k = 20$ in the case of the latter strategy.

| | step length | step width | step time | forward velocity | area of BoA $(\cdot 10^{-3})$ | $\phi$ range (rad) |
|---|---|---|---|---|---|---|
| *beta* | $0.4989 \pm 0.0178$ | $0.0606 \pm 0.0242$ | $1.8901 \pm 0.0274$ | $0.3666 \pm 0.0032$ | $0.3862 \pm 0.2498$ | $[-0.04 \pm 0.03, 0.03 \pm 0.02]$ |
| *ratio-beta* (k=17.8389) | $0.4631 \pm 0.0114$ | $0.0558 \pm 0.0224$ | $1.8384 \pm 0.0166$ | $0.3593 \pm 0.0024$ | $4.4 \pm 2.5$ | $[-0.29 \pm 0.18, 0.41 \pm 0.17]$ |
| *ratio-beta* (k=15) | $0.4975 \pm 0.001$ | $0.0664 \pm 0.0222$ | $2.0095 \pm 5 \cdot 10^{-4}$ | $0.3547 \pm 7 \cdot 10^{-4}$ | $6 \pm 2$ | $[-0.34 \pm 0.16, 0.59 \pm 0.04]$ |
| *ratio-beta* (k=20) | $0.4439 \pm 0.0092$ | $0.0578 \pm 0.197$ | $1.7398 \pm 0.016$ | $0.3621 \pm 0.0013$ | $4 \pm 3.2$ | $[-0.29 \pm 0.23, 0.33 \pm 0.25]$ |

Table 4.1: Gait characteristics of stable patterns

Even though there were multiple patterns of 3D walking with 2 different leg strategies that exhibited stable walking, neither strategy was able to attain directional stability of the model. There was neutral stability along the lateral direction, thus perturbations that affected this dimensions of the phase space vector resulted in a change of the walking direction for the model. Two examples are shown in Figures 4.6 and Figure 4.7, where a lateral push and a pull respectively ($v_{z,dist} = \pm 0.1$) during transversal plane orientation of the left leg are simulated. This type of force disturbance differed from the one proposed above, where the velocity angle was perturbed to simulate an applied brief force on the centre of mass. Rotating the velocity vector to simulate such a perturbation kept the energy level $E$ equal to its original value. Adding a lateral component to the velocity vector altered the energy level, which remained constant afterwards since the model did not include a damping mechanism. This test was conducted in order to investigate the model's performance on an energy level, while utilising a leg strategy that proved to be stable on another level. The magnitude of the applied lateral velocity was $29\%$ of the forward walking speed and it was tested on the most robust found pattern, with $k = 15, \theta = 1.2749\ rad, \beta = 0.0843\ rad$.

It is worth noting that even though this pattern was asymmetric in the sense that the

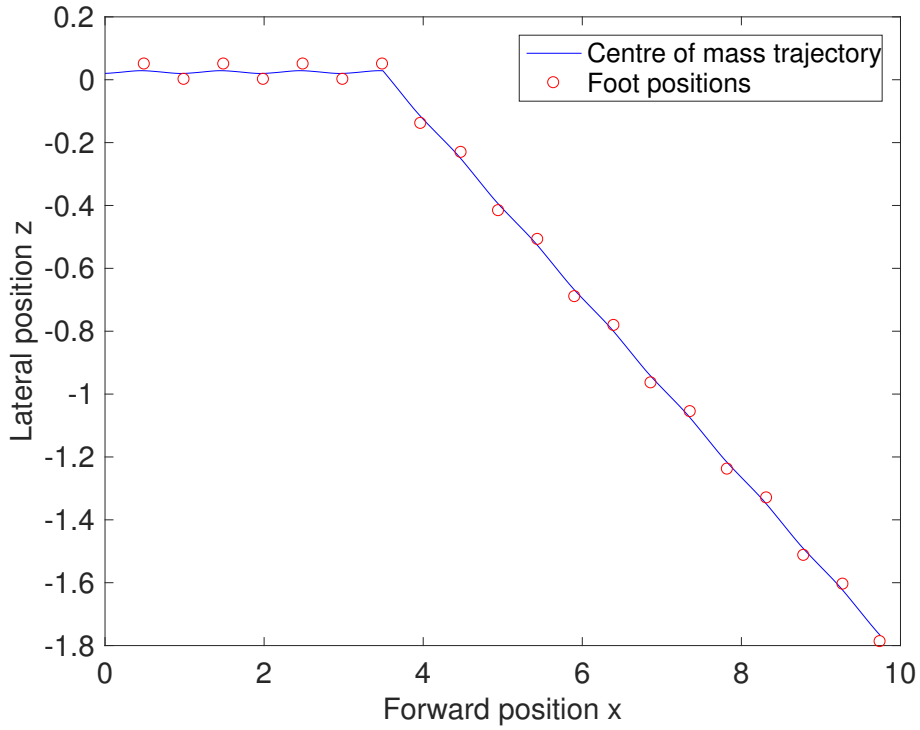


(a) Horizontal plane

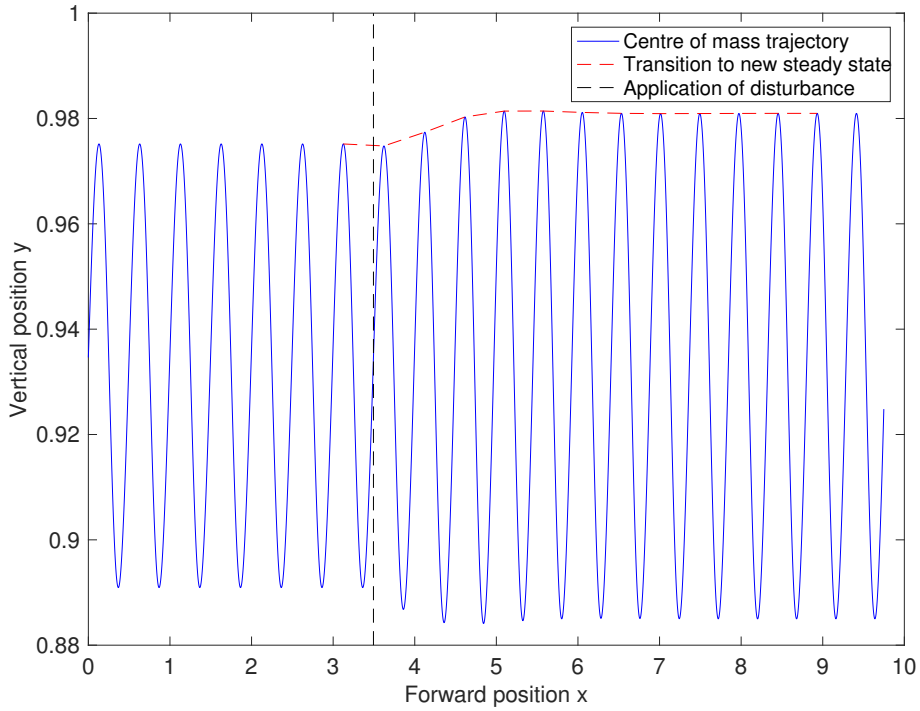


(b) Saggital plane

Figure 4.6: Performance of the most robust pattern under a lateral push $v_{z,dist} = -0.1$

ground reaction force profiles could not be mirrored around the middle of each step, the forces were identical on both legs, as it can be seen in Figure 4.8.

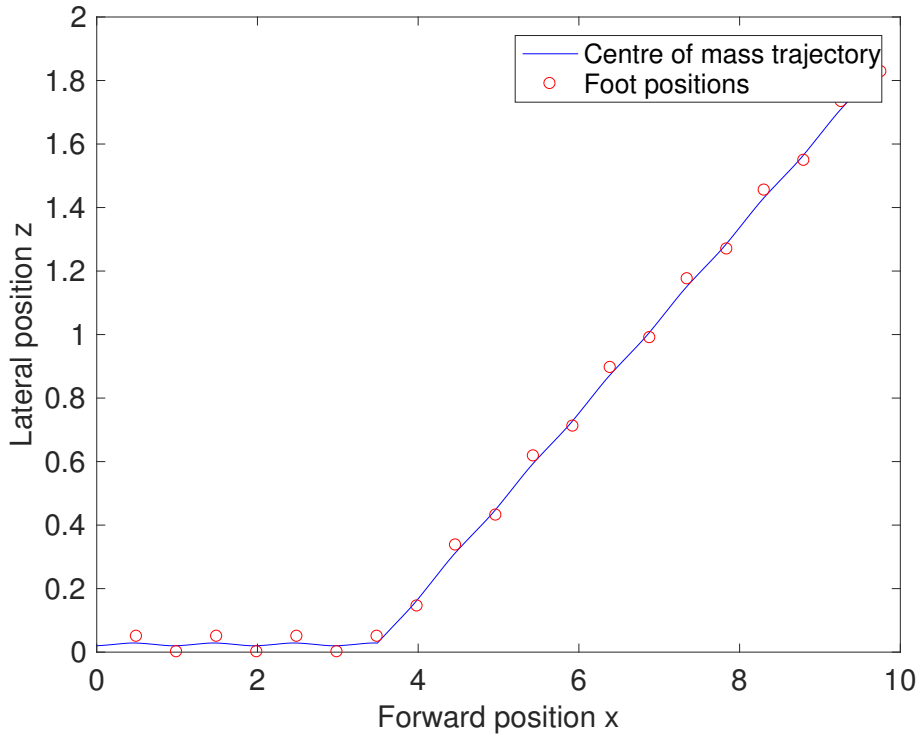


(a) Horizontal plane

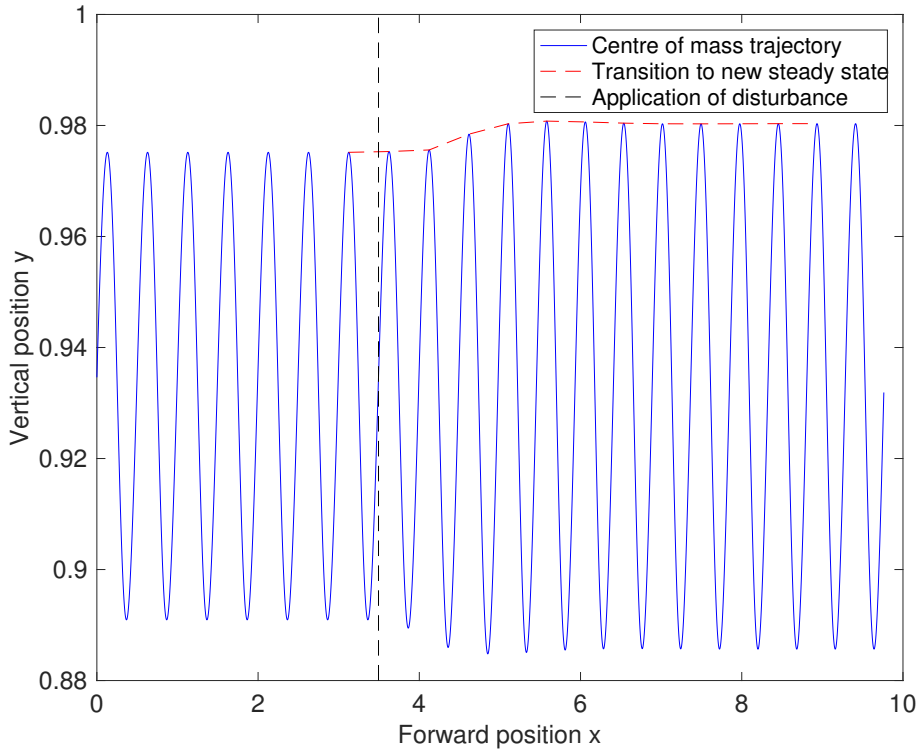


(b) Saggital plane

Figure 4.7: Performance of the most robust pattern under a lateral push $v_{z,dist} = 0.1$

Deviations from the walking direction were finally calculated for the most robust pattern within its 2D basin of attraction along the $y$ and $z$ dimensions. In this way, the inability

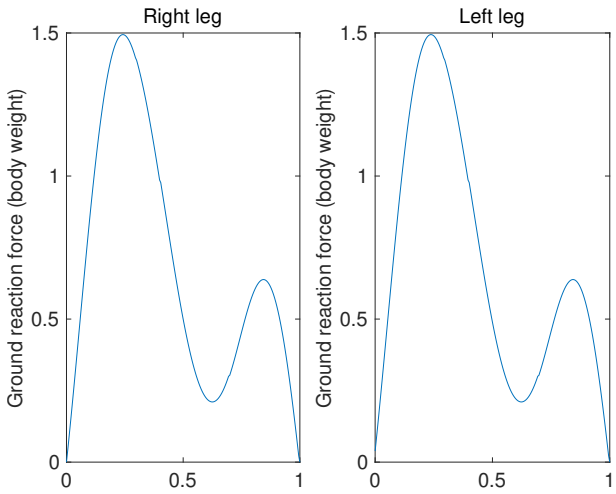


Figure 4.8: Ground reaction force profiles on both legs for the most robust identified pattern

of the model to attain a specified walking direction under spatial perturbations of the foot's position on the ground was quantified. Figure 4.9 includes the results.

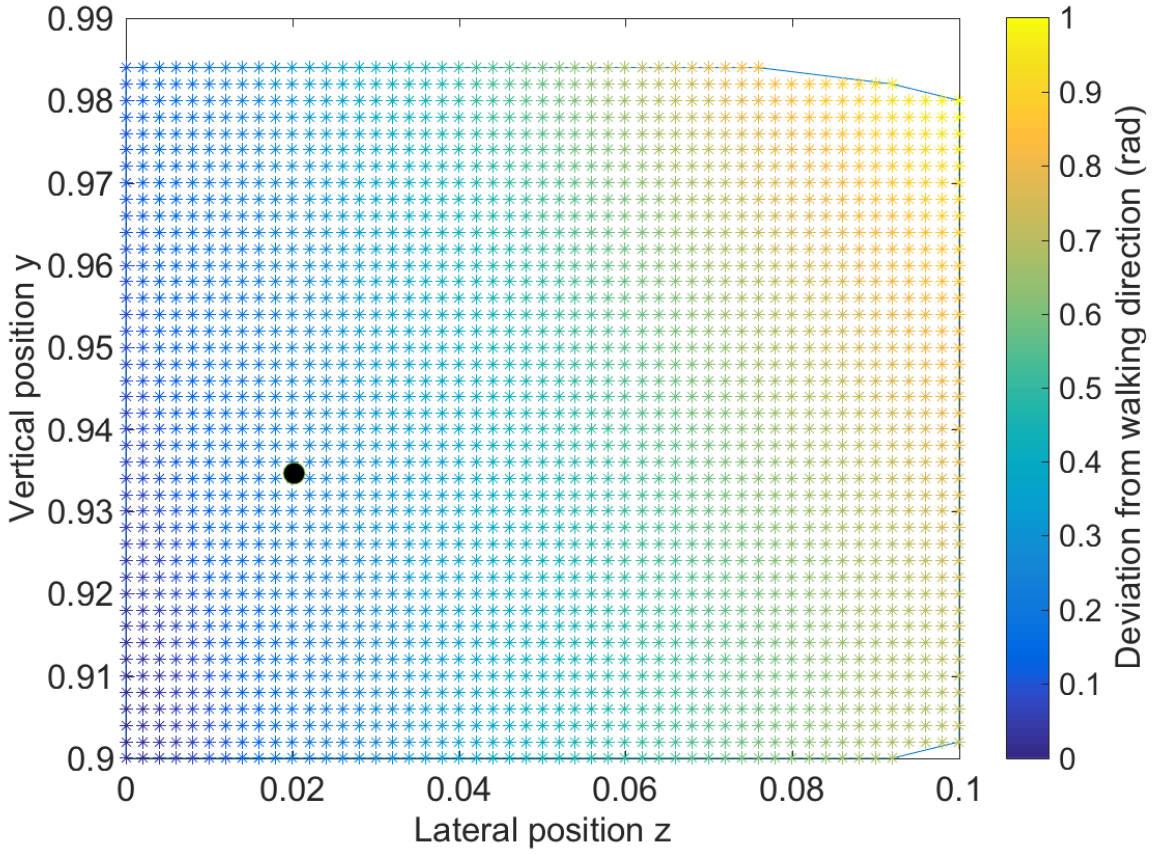


Figure 4.9: Basin of attraction of most robust pattern with calculated deviations from the initial walking direction. Black dot represents the stable node.

# Chapter 5

# Discussion

The two questions that motivated the present project were: is it possible for a 3D model with compliant legs to walk stably under simple open-loop control? and if stable walking configurations are possible, do they explain the observed behaviour of humans walking during constant speed walking in a straight line, even under perturbations? It has been argued in the **Literature Review** chapter that the 3D bipedal spring-mass model of Figure 2.1 was a suitable candidate to address both questions. The benefits and the limitations of this model in conjunction with the methods chosen to analyse it and the produced results of the previous chapters are discussed below. The discussion treated the two questions separately, as the first one sought to introduce guidelines for the design and control of artificial systems, while the second one concerned the origin of control during walking in humans and the extent at which this control is related to passive dynamics of the body.

## 5.1 Robust walking with a passive dynamics 3D model

The task of leading the 3D bipedal spring-mass model to steady state periodic walking belonged to the category of underactuated control. There were 4 dimensions of interest to be controlled, expressed in the phase space vector $s$ (equation 3.27) and 2 control variables, $\theta = f(\dot{q}, q)$ and $\beta = g(\dot{q}, q)$. The inherent simplicity of the model limited the number of available system variables to the position and velocity of the centre of mass, $\dot{q}, q$, that constituted the state space representation of the model. Three options were considered for each of the $f, g$ functions (equations 3.28 to 3.33) that utilized the centre of mass information to different extents. Pairs of $f, g$ functions formed control

strategies. The range of these strategies in terms of the required information varied from no information at all in the case of constant leg angles in a world reference frame (equations 3.28 and 3.31) to adjusting the leg according to the velocity (equations 3.29, 3.30, 3.32) or both velocity and position (equation 3.33) of the centre of mass. These strategies were chosen because they have led to promising results in similar models of locomotion (Peuker et al. (2012)) or have closely matched experimental data (Hof et al. (2007)). A $10^{th}$ strategy consisted of constant step length and width during every step and calculated the leg angles indirectly.

Two strategies were successful in attaining stability of the model. *Beta* strategy (Figure 4.1), which fixed the $\theta$ angle based on a world reference frame and adjusted $\beta$ at a fixed angle laterally from the velocity vector (equation 3.32), and *ratio-beta* (Figure 4.2) that used the same function for $\beta$ and placed $\theta$ below the velocity vector, at an angle that was calculated as a ratio of the total angle between velocity and gravity vectors (3.30). Between the two, *ratio-beta* strategy clearly exhibited superior robustness, with areas of basin of attraction an order of magnitude larger than the ones of *beta* in the $z, y$ plane and much larger ranges of perturbed velocity angles $\phi$ (Table 4.1). Figure 4.3 included a clearer comparison between a pair of walking patterns, one from each strategy, that exhibited the smallest differences in step length, width and time among all possible pairs. Even though these apparent walking parameters were very similar, the stability of each pattern was noticeably different.

The additional requirement of *ratio-beta* was the sensing of the vertical velocity component $v_y$ for the adjustment of $\theta$. It has been argued that this cost was less important than the increased robustness of the *ratio-beta* strategy, because stability was considered of higher priority than energy consumption (Birn-Jeffery et al. (2014), Ferris et al. (1999)), as lack of stability hinders any movement and could cause damages with greater costs. Additional sensing, whether it is performed by electronics or mechanical components, implies increased susceptibility to inaccurate measurements. However, the ranges of the control variables among the found patterns was sufficient to allow for small amounts of input noise from velocity sensing or motor control of the leg angles. Even though more patterns were found for *beta* (29 compared to 19 for *ratio-beta*), these ranges were very similar in both cases. Particularly in the case of *ratio-beta* strategy, it can be noticed from Figures 4.2, 4.4 and 4.5 that the most stable patterns, drawn with a green colour, included all other stable nodes in their basins of attraction in the $z, y$ plane of the figures. Thus, any deviation of the leg angle values in one of those patterns, that is within the limits of the $\theta, \beta$ values of the included patterns, would still result in asymptotic stability. This statement holds for deviations in a single step. When inaccurate

leg placement occurs through multiple steps, asymptotic stability holds if the deviated leg angle values correspond to stable nodes, whose basins of attraction include a sufficient number of other stable nodes to allow for further inaccurate leg placements. This condition held for *ratio-beta*, as there was a clear dependence of the area of the basin from $\theta$ and $\beta$ (Figures 4.2(b), 4.4(b), 4.5(b)), which was not apparent in the case of *beta* strategy (Figure 4.1(b)). Consequently, the most stable nodes, that included all other stable nodes in their basins, corresponded to walking patterns with neighbouring $\theta, \beta$ values for *ratio-beta* strategy, thus enlarging the angle ranges that ensure stability.

This project work included only a partial map of the locations of stable nodes in phase space, as the initial guesses of the Newton-Raphson algorithm for the solution of equation 3.36 exclusively included walking patterns with identical force profiles on both legs. This choice was made in order to avoid patterns that resulted in uneven loading between the two legs, as shown in Figure 3.4(b), and to manage the project time more efficiently by reducing the size of the search space. The outcome of this approach was to identify a leg placement strategy, *ratio-beta*, with considerably larger robustness than other simple strategies, so that focus would be drawn to it in an extended future investigation of its phase space. By extending the ranges of every component of the initial vector $s_0$ (equation 3.27), additional stable nodes can be located, increasing the ranges of allowable $\theta, \beta$ values for the nodes whose basins of attraction include an increased number of other nodes. This is the general form of the statement in the previous paragraph and enhances the argument that accurate leg placement is not necessary in the proposed model. Meaningful ranges for the velocity vector angles of the state space vector are $\phi_0, \psi_0 \in [-\frac{\pi}{2}, \frac{\pi}{2}]$, otherwise the model would walk backwards. For $y, z$ the basins of attraction for the *ratio-beta* strategy showed that stable walking was possible throughout the proposed ranges and further expansion of those ranges would be possible, while always keeping the maximum leg length equal to its natural length. The complete ranges of physically plausible initial conditions would result in more asymmetric patterns. However, asymmetric patterns with the same loading conditions on both legs were found, as was the case of the most robust pattern in Figure 4.8, which would not complicate the structural analysis and material choices for the construction and maintanance of the legs of a bipedal robot. Determining the positions of all possible stable nodes, their respective $\theta, \beta$ values and basins of attraction, would allow the calculation of all reachable states from each node. This, in turn, could result in the formulation of a deadbeat control strategy, where the system would converge to a desired steady state after the minimum amount of steps instead of asymptotically, while using the phase space as a map of the parameters of each consecutive step, similar to the one proposed in Vejdani et al. (2015) for the 2D walking model.

In terms of the design parameters, it was shown that a non-dimensional stiffness of $k = 15$ resulted in the most robust walking patterns, as compared to $k = 17.8389$ and $k = 20$. This result was in agreement with a stability analysis performed on the 2D version of the investigated model that captured only the saggital plane dynamics (Rummel et al. (2010)). Table 4.1 noted the steady decrease in the size of the basins of attraction of the identified stable nodes as stiffness increased. Particularly in the case of $k = 20$, some nodes had too small basins to be captured by the grid of perturbed initial conditions (blue nodes in Figure 4.5(a)).

The development of a bipedal robot that resembles the 3D spring-mass model and applies the *ratio-beta* strategy was encouraged by the result of this project. Particularly after producing a more detailed map of the phase space with more stable node positions, the need for accurate leg angle adjustments would decrease, as discussed in the previous paragraphs. Furthermore, it would be valuable to test how the predicted model performance translates into a real-world application. The disadvantage of the strategy was its neutral stability along the horizontal plane, as any arbitrary perturbation that affected the horizontal plane dynamics resulted in changes of the walking direction. This was an inherent feature of both *beta* and *ratio-beta* strategies, as the calculation of the lateral leg angle $\beta$ was based on an egocentric reference frame that was formed by the centre of mass velocity vector. Nevertheless, asymptotic stability was exhibited in all other dimensions of the phase space. Two examples that supported this claim were included in Figures 4.6 and 4.7, where a relatively large lateral perturbation ( $29$% of the forward walking speed) was applied in both directions. An approximate number of $7$ steps after the disturbance was sufficient to return to steady state walking in both cases. Asymptotic stability was achieved, even though the energy level of the conservative system changed into a value that was not investigated. Naturally, the magnitude of the centre of mass oscillation on the saggital plane increased as well, highlighting the need for some active control component to regulate energy changes on the actual robot. Perturbations to the position of the foot also cause a change to the walking direction. These were modelled as perturbations along the $y, z$ coordinates. In the case of the most robust pattern, the deviations of walking direction caused by these perturbations were calculated and depicted in Figure 4.9. The maximum value was $1\ rad$ and there was a clear dependence of the angle of deviation from the $z$ coordinate. A mirrored figure with negative $z$ and deviation angle values would be the outcome of applying the same perturbation on the right leg during the instance of transversal plane orientation. The boundaries of stable walking together with the deviations that might be caused within them were directly calculated. This strategy is proposed to be used in steady state walking to minimise energy expenditure via limited sensory and motor

demands, while a higher level control process would be used to detect and correct deviations from the desired walking direction. The necessary operational boundaries of this higher level process would be the direct result of the calculated deviations of Figure 4.9.

## 5.2 Passive dynamics of human walking

The second aim of the present project was to investigate whether the 3D spring-mass model with simple leg strategies could match experimental findings of human walking. According to Table 4.1, the gait parameters of the model did not match the preferred values for human walking. Step length during human walking has been observed to follow the equation $d \approx u^{0.42}$ (Kuo (2001)) and step width is typically $w \approx 0.13$ (Donelan et al. (2001)) in the non-dimensional case. However, it was shown in Geyer et al. (2006) that the model matched ground reaction force profiles, centre of mass trajectories and kinematic-potential energy exchanges using stiffness values that were lower than the measured leg stiffnesses on humans. This fact imposed a limit on the ability of the model to quantitatively capture both gait parameters and centre of mass dynamics and energetics of human walking.

Even though there were limits to matching measured values of step length and width, the model exhibited qualitative value in terms of the control of leg placement. The main hypothesis from the biomechanics literature, as discussed in the **Literature Review** chapter, was that the centre of mass position and velocity were important factors for correct leg placement and the measured step width on humans depends linearly on both variables. Rewriting the original version of equation 3.33 from the literature

$$w = z_{TD} + \frac{\dot{z}_{TD}}{\omega_0} + b \tag{5.1}$$

$z_{TD}, \dot{z}_{TD}$ denoted the lateral position and velocity of the centre of mass during touchdown, $\omega_0 = \sqrt{\frac{g}{l_r}}$ corresponded to the eigenfrequency of the legs and $b$ was an added value. Hof et al. (2010) noted that $b$ had an important standard deviation, which resulted in non-precise leg placement. The strategy that led to stable walking in the model applied equation 3.32 for lateral leg placement. The calculated step width, in the dimensional case to match equation 5.1 and with $\dot{z}_{TD} = v_{z,TD}, \dot{x}_{TD} = v_{x,TD}$, according

to this strategy was

$$
\begin{aligned}
w &= z_{TD} + l_r \cos\theta \sin\beta, \quad \text{where } \beta = \tan^{-1}\left(\frac{\dot{z}_{TD}}{\dot{x}_{TD}}\right) + \beta_c, \quad \beta_c \in [0.03, 0.12] \text{ radians} \\
&= z_{TD} + l_r \cos\theta \sin\left[\tan^{-1}\left(\frac{\dot{z}_{TD}}{\dot{x}_{TD}}\right) + \beta_c\right] \\
&= z_{TD} + l_r \cos\theta \left(\frac{\dot{z}_{TD}\cos\beta_c + \dot{x}_{TD}\sin\beta_c}{\sqrt{\dot{x}_{TD}^2 + \dot{z}_{TD}^2}}\right)
\end{aligned} \tag{5.2}
$$

The relationship between lateral and forward components of velocity was $\dot{z} \approx 0.02\dot{x}$ on average throughout a stride and among all the stable patterns found. The mean values of forward velocity for each strategy were presented in Table 4.1. Even though lateral velocity was a larger ratio of forward velocity during touch-down, which was the event of interest in terms of leg placement control, it did not exceed a value of $0.025\dot{x}_{TD}$. Thus it was safely assumed that $\dot{x}^2 >> \dot{z}^2 \Rightarrow v_h = \sqrt{\dot{x}^2 + \dot{z}^2} = \sqrt{\dot{x}^2} = \dot{x}$ at any instance including the touch-down event, as $\dot{x} > 0$ for forward walking. When applied on equation 5.2, this assumption yielded

$$
\begin{aligned}
w &= z_{TD} + \frac{\dot{z}_{TD}}{\frac{\dot{x}_{TD}}{l_r \cos\theta \cos\beta_c}} + l_r \cos\theta \sin\beta_c \\
&= z_{TD} + \frac{\dot{z}_{TD}}{\frac{\dot{x}_{TD}}{l_h}} + l_p
\end{aligned} \tag{5.3}
$$

The lengths $l_h$ and $l_p$ were projections of the leg along and perpendicular to the horizontal velocity vector $v_h$ respectively. These are drawn in Figure 5.1 for clarity.

There was an apparent similarity between equations 5.1 and 5.3. However, there was no evidence in the literature as to why the equations $\omega_0 = \frac{\dot{x}_{TD}}{l_h}$ and $b = l_p$ should hold. The same strategy for lateral leg placement that produced equation 5.3 was applied on the 3D model in Maus and Seyfarth (2014) to predict the circular change of walking direction that was observed in people without external visual references. Based on this study and on the qualitative similarity of equations 5.1 and 5.3, it can be stated that humans partly rely on the same open-loop strategies of the form 3.32 to adjust the lateral position of the leg that have led to stable walking in the 3D spring-mass model. Furthermore, the model agreed with the hypothesis presented in the **Literature Review** from the experimental literature that centre of mass position and velocity are key factor for the control of stability. As a matter of fact, the successful strategies depended exclusively on the kinematics of the centre of mass and this egocentric nature made them susceptible to perturbations that affected the walking direction. This fact indicated that humans could only partly rely on the passive dynamics of an abstract model that

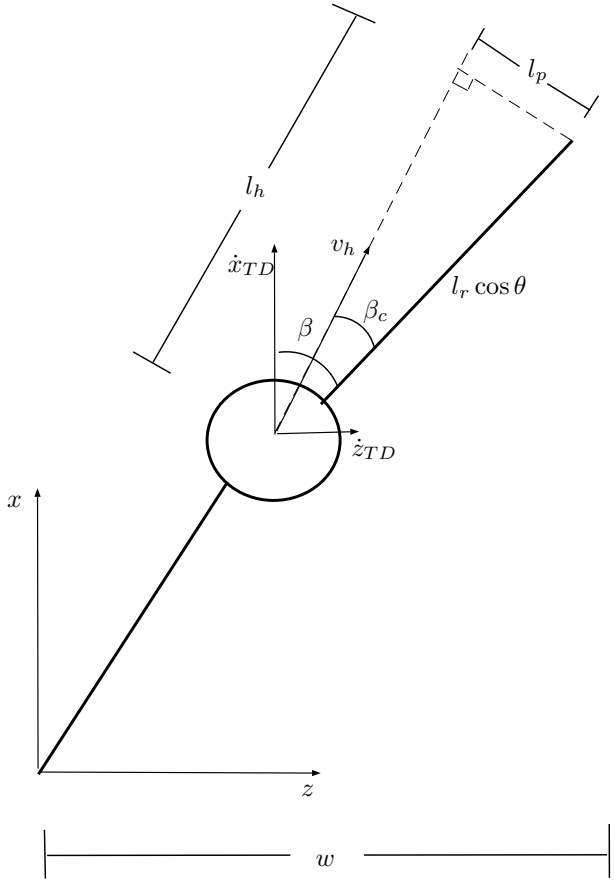


Figure 5.1: Horizontal plane including $l_h$ and $l_p$

includes the legs and the centre of mass. A higher level control process relying on external references has to be present in order to maintain a desired walking direction.

In order to investigate the passive dynamics of human walking more thoroughly, the proposed leg placement strategies, *beta* and more importantly *ratio-beta*, have to be tested under perturbations. This can not be achieved straightforwardly, by applying external lateral pushes/pulls or perturbations to the initial conditions vector as these approaches resulted in changes of the walking direction, as it was observed in Figures 4.6, 4.7 and 4.9. Changes to the energy level could be employed to simulate external perturbations. If the change of step width would be proportional to the energy level change, then the model would agree with the experimental observation that step width varies in proportion to lateral perturbations, as these perturbations mainly affect the velocity and step width depends linearly on lateral velocity (equation 5.1). However, the forward velocity $v_x$ of the model has to remain constant in order to match energy level changes to external perturbations, which can not be achieved with the current model when all other system variables remain equal to their values before the energy change as well. This limitation was imposed because the model was conservative

(equation 3.23) and both position and velocity were included in the dynamics equations 3.8 to 3.13 and varied during integration. In an experimental set-up, this was achieved by walking on a treadmill with a predetermined speed, whereas the model has to be reformulated to conduct perturbation simulations.

# Chapter 6

# Bibliography

R. McN. Alexander. Three uses for springs in legged locomotion. *The International Journal of Robotics Research*, 9(2):53–61, 1990. doi: 10.1177/027836499000900205. URL http://dx.doi.org/10.1177/027836499000900205.

Richard Altendorfer, Daniel E Koditschek, and Philip Holmes. Stability analysis of legged locomotion models by symmetry-factored return maps. *International Journal of Robotics Research*, 23:10–11, 2004.

Catherine E. Bauby and Arthur D. Kuo. Active control of lateral balance in human walking. *Journal of Biomechanics*, 33(11):1433–1440, 2000. doi: 10.1016/S0021-9290(00)00101-9. URL http://dx.doi.org/10.1016/S0021-9290(00)00101-9.

Aleksandra V. Birn-Jeffery, Christian M. Hubicki, Yvonne Blum, Daniel Renjewski, Jonathan W. Hurst, and Monica A. Daley. Don't break a leg: running birds from quail to ostrich prioritise leg safety and economy on uneven terrain. *Journal of Experimental Biology*, 217(21):3786–3796, 2014. ISSN 0022-0949. doi: 10.1242/jeb.102640. URL http://jeb.biologists.org/content/217/21/3786.

R. Blickhan. The spring-mass model for running and hopping. *Journal of Biomechanics*, 22(11):1217–1227, 2017/03/30 1989. doi: 10.1016/0021-9290(89)90224-8. URL http://dx.doi.org/10.1016/0021-9290(89)90224-8.

Reinhard Blickhan, Andre Seyfarth, Hartmut Geyer, Sten Grimmer, Heiko Wagner, and Michael Günther. Intelligence by mechanics. *Philosophical Transactions of the Royal Society of London A: Mathematical, Physical and Engineering Sciences*, 365(1850):199–220, 2007. ISSN 1364-503X. doi: 10.1098/rsta.2006.1911. URL http://rsta.royalsocietypublishing.org/content/365/1850/199.

B. G. Buss, A. Ramezani, K. Akbari Hamed, B. A. Griffin, K. S. Galloway, and J. W. Grizzle. Preliminary walking experiments with underactuated 3d bipedal robot marlo. In *2014 IEEE/RSJ International Conference on Intelligent Robots and Systems*, pages 2529–2536, Sept 2014. doi: 10.1109/IROS.2014.6942907.

G A Cavagna and R Margaria. Mechanics of walking. *Journal of Applied Physiology*, 21 (1):271–278, 1966. ISSN 8750-7587. URL http://jap.physiology.org/content/21/1/271.

Giovanni A Cavagna, Norman C Heglund, and C Richard Taylor. Mechanical work in terrestrial locomotion: two basic mechanisms for minimizing energy expenditure. *American Journal of Physiology-Regulatory, Integrative and Comparative Physiology*, 233(5):R243–R261, 1977.

Steve Collins, Andy Ruina, Russ Tedrake, and Martijn Wisse. Efficient bipedal robots based on passive-dynamic walkers. *Science*, 307(5712):1082–1085, 2005. ISSN 0036-8075. doi: 10.1126/science.1107799. URL http://science.sciencemag.org/content/307/5712/1082.

J M Donelan, R Kram, and A D Kuo. Mechanical and metabolic determinants of the preferred step width in human walking. *Proceedings of the Royal Society B: Biological Sciences*, 268(1480):1985–1992, 10 2001.

Daniel P Ferris, Kailine Liang, and Claire T Farley. Runners adjust leg stiffness for their first step on a new running surface. *Journal of Biomechanics*, 32(8):787 – 794, 1999. ISSN 0021-9290. doi: http://dx.doi.org/10.1016/S0021-9290(99)00078-0. URL http://www.sciencedirect.com/science/article/pii/S0021929099000780.

T Fukunaga, K Kubo, Y Kawakami, S Fukashiro, H Kanehisa, and C N Maganaris. In vivo behaviour of human muscle tendon during walking. *Proceedings of the Royal Society B: Biological Sciences*, 268(1464):229–233, 2001. doi: 10.1098/rspb.2000.1361. URL http://www.ncbi.nlm.nih.gov/pmc/articles/PMC1088596/.

R.J. Full and D.E. Koditschek. Templates and anchors: neuromechanical hypotheses of legged locomotion on land. *Journal of Experimental Biology*, 202(23):3325–3332, 1999. ISSN 0022-0949. URL http://jeb.biologists.org/content/202/23/3325.

Hartmut Geyer, Andre Seyfarth, and Reinhard Blickhan. Compliant leg behaviour explains basic dynamics of walking and running. *Proceedings of the Royal Society B: Biological Sciences*, 273(1603):2861–2867, 11 2006. doi: 10.1098/rspb.2006.3637. URL http://www.ncbi.nlm.nih.gov/pmc/articles/PMC1664632/.

A. L. Hof, S. M. Vermerris, and W. A. Gjaltema. Balance responses to lateral perturbations in human treadmill walking. *Journal of Experimental Biology*, 213(15): 2655–2664, 2010. ISSN 0022-0949. doi: 10.1242/jeb.042572. URL http://jeb.biologists.org/content/213/15/2655.

At L. Hof, Renske M. van Bockel, Tanneke Schoppen, and Klaas Postema. Control of lateral balance in walking. *Gait & Posture*, 25(2):250–258, 2017/03/30 2007. doi: 10.1016/j.gaitpost.2006.04.013. URL http://dx.doi.org/10.1016/j.gaitpost.2006.04.013.

Philip Holmes, Robert J. Full, Dan Koditschek, and John Guckenheimer. The dynamics of legged locomotion: Models, analyses, and challenges. *SIAM Review*, 48(2):207–304, 2006. doi: 10.1137/S0036144504445133. URL https://doi.org/10.1137/S0036144504445133.

Yildirim Hurmuzlu, Frank Génot, and Bernard Brogliato. Modeling, stability and control of biped robots—a general framework. *Automatica*, 40(10):1647 – 1664, 2004. ISSN 0005-1098. doi: http://dx.doi.org/10.1016/j.automatica.2004.01.031. URL http://www.sciencedirect.com/science/article/pii/S0005109804000998.

Auke J. Ijspeert. Biorobotics: Using robots to emulate and investigate agile locomotion. *Science*, 346(6206):196–203, 2014. ISSN 0036-8075. doi: 10.1126/science.1254486. URL http://science.sciencemag.org/content/346/6206/196.

Shuuji Kajita and Bernard Espiau. *Springer Handbook of Robotics*. Springer Berlin Heidelberg, Berlin, Heidelberg, 2008. ISBN 978-3-540-30301-5.

Arthur D. Kuo. Stabilization of lateral motion in passive dynamic walking. *The International Journal of Robotics Research*, 18(9):917–930, 1999. doi: 10.1177/02783649922066655. URL http://dx.doi.org/10.1177/02783649922066655.

Arthur D. Kuo. A simple model of bipedal walking predicts the preferred speed–step length relationship. *Journal of Biomechanical Engineering*, 123(3):264–269, 01 2001.

Horst-Moritz Maus and Andre Seyfarth. Walking in circles: a modelling approach. *Journal of The Royal Society Interface*, 11(99), 2014. ISSN 1742-5689. doi: 10.1098/rsif.2014.0594. URL http://rsif.royalsocietypublishing.org/content/11/99/20140594.

Tad McGeer. Passive dynamic walking. *Int. J. Rob. Res.*, 9(2):62–82, March 1990. ISSN 0278-3649. doi: 10.1177/027836499000900206. URL http://dx.doi.org/10.1177/027836499000900206.

Andreas Merker, Dieter Kaiser, and Martin Hermann. Numerical bifurcation analysis of the bipedal spring-mass model. *Physica D: Nonlinear Phenomena*, 291:21 – 30, 2015. ISSN 0167-2789. doi: http://dx.doi.org/10.1016/j.physd.2014.09.010. URL http://www.sciencedirect.com/science/article/pii/S0167278914001924.

Lars I. E Oddsson, III Wall, Conrad, Michael D McPartland, David E Krebs, and Carole A Tucker. Recovery from perturbations during paced walking. *Gait & Posture*, 19(1): 24–34, 2017/03/30 2004. doi: 10.1016/S0966-6362(03)00008-0. URL http://dx.doi.org/10.1016/S0966-6362(03)00008-0.

Haris Organtzidis. Control for stability of bipedal locomotion: Research plan. Coursework submitted for the Robotics Research Prepeartion unit at the University of Bristol, March 2017.

Thomas S. Parker and Leon O. Chua. *Practical Numerical Algorithms for Chaotic Systems*. Springer-Verlag New York, Inc., New York, NY, USA, 1989. ISBN 0-387-96689-7.

Frank Peuker, Christophe Maufroy, and André Seyfarth. Leg-adjustment strategies for stable running in three dimensions. *Bioinspiration & Biomimetics*, 7(3):036002, 2012. URL http://stacks.iop.org/1748-3190/7/i=3/a=036002.

Friedrich Pfeiffer and Hirochika Inoue. Walking: technology and biology. *Philosophical Transactions of the Royal Society of London A: Mathematical, Physical and Engineering Sciences*, 365(1850):3–9, 2007. ISSN 1364-503X. doi: 10.1098/rsta.2006.1918. URL http://rsta.royalsocietypublishing.org/content/365/1850/3.

Jerry Pratt, Chee-Meng Chew, Ann Torres, Peter Dilworth, and Gill Pratt. Virtual model control: An intuitive approach for bipedal locomotion. *The International Journal of Robotics Research*, 20(2):129–143, 2001. doi: 10.1177/02783640122067309. URL http://dx.doi.org/10.1177/02783640122067309.

Marc H. Raibert. *Legged Robots That Balance*. Massachusetts Institute of Technology, Cambridge, MA, USA, 1986. ISBN 0-262-18117-7.

Siavash Rezazadeh, Christian Hubicki, Mikhail Jones, and Andy Abate. Spring-mass walking with atrias in 3d: Robust gait control spanning zero to 4.3 kph on a heavily underactuated bipedal robot. 2015.

J. Rummel, Y. Blum, H. M. Maus, C. Rode, and A. Seyfarth. Stable and robust walking with compliant legs. In *2010 IEEE International Conference on Robotics and Automation*, pages 5250–5255, May 2010. doi: 10.1109/ROBOT.2010.5509500.

Y. Sakagami, R. Watanabe, C. Aoyama, S. Matsunaga, N. Higaki, and K. Fujimura. The intelligent asimo: system overview and integration. In *IEEE/RSJ International Conference on Intelligent Robots and Systems*, volume 3, pages 2478–2483 vol.3, 2002. doi: 10.1109/IRDS.2002.1041641.

Koushil Sreenath, Hae-Won Park, Ioannis Poulakakis, and J W Grizzle. A compliant hybrid zero dynamics controller for stable, efficient and fast bipedal walking on mabel. *Int. J. Rob. Res.*, 30(9):1170–1193, August 2011. ISSN 0278-3649. doi: 10.1177/0278364910379882. URL http://dx.doi.org/10.1177/0278364910379882.

Steven H. Strogatz. *Nonlinear dynamics and chaos : with applications to physics, biology, chemistry, and engineering*. Second edition. Boulder, CO : Westview Press, a member of the Perseus Books Group, 2015, 2015.

H. R. Vejdani, A. Wu, H. Geyer, and J. W. Hurst. Touch-down angle control for spring-mass walking. In *2015 IEEE International Conference on Robotics and Automation (ICRA)*, pages 5101–5106, May 2015. doi: 10.1109/ICRA.2015.7139909.

M. Vlutters, E. H. F. van Asseldonk, and H. van der Kooij. Center of mass velocity-based predictions in balance recovery following pelvis perturbations during human walking. *Journal of Experimental Biology*, 219(10):1514–1523, 2016. ISSN 0022-0949. doi: 10.1242/jeb.129338. URL http://jeb.biologists.org/content/219/10/1514.

Yang Wang and Manoj Srinivasan. Stepping in the direction of the fall: the next foot placement can be predicted from current upper body state in steady-state walking. *Biology Letters*, 10(9), 2014. ISSN 1744-9561. doi: 10.1098/rsbl.2014.0405. URL http://rsbl.royalsocietypublishing.org/content/10/9/20140405.

Albert Wu and Hartmut Geyer. The 3-d spring-mass model reveals a time-based deadbeat control for highly robust running and steering in uncertain environments. pages 1–11, 01 2013.

Xiaodong Zhou and Shusheng Bi. A survey of bio-inspired compliant legged robot designs. *Bioinspiration & Biomimetics*, 7(4):041001, 2012. URL http://stacks.iop.org/1748-3190/7/i=4/a=041001.

# Appendices

# Appendix A

# Ethical Review Checklist

University of the West of England
BRISTOL

**Faculty of Environment & Technology**
**Faculty Research Ethics Committee (FET FREC)**

**ETHICAL REVIEW CHECKLIST FOR UNDERGRADUATE AND POSTGRADUATE MODULES**
*Please provide project details and complete the checklist below.*

**Project Details:**

| | |
|---|---|
| **Module name** | **Dissertation (masters)** |
| **Module code** | **UFMED4-60-M** |
| **Module leader** | **Dr Maryam Atoofi** |
| **Project Supervisor** | **Dr JF Burn** |
| **Proposed project title** | **Leg placement control based on passive dynamics of a 3D walking model** |

**Applicant Details:**

| | |
|---|---|
| **Name of Student** | Charalampos Organtzidis |
| **Student Number** | 16042854 |
| **Student's email address** | organtzh@gmail.com |

| | CHECKLIST QUESTIONS | Y/N | Explanation |
|---|---|---|---|
| 1. | Does the proposed project involve **human tissue, human participants, environmental damage, the NHS, or data gathered outside the UK**? | N | *If the answer to this is 'N' then no further checks in the list need to be considered.* |
| 2. | Will participants be clearly asked to give consent to take part in the research and informed about how data collected in the research will be used? | | |
| 3. | If they choose, can a participant withdraw at any time (prior to a point of "no return" in the use of their data)? Are they told this? | | |
| 4. | Are measures in place to provide confidentiality for participants and ensure secure management and disposal of data collected from them? | | |

| | CHECKLIST QUESTIONS | Y/N | Explanation |
|---|---|---|---|
| 5. | Does the study involve people who are particularly vulnerable or unable to give informed consent (eg, children or people with learning difficulties)? | | |
| 6. | Could your research cause stress, physical or psychological harm to anyone, or environmental damage? | | |
| 7. | Could any aspects of the research lead to unethical behaviour by participants or researchers (eg, invasion of privacy, deceit, coercion, fraud, abuse)? | | |
| 8. | Does the research involve the NHS or collection or storage of human tissue (includes anything containing human cells, such as saliva and urine)? | | |

Your explanations should indicate briefly for Qs 2-4 how these requirements will be met, and for Qs 5-8 what the pertinent concerns are.

- If Qs 2-4 are answered Yes (Y) and Qs 5-8 are answered No (N), no further reference to the Research Ethics Committee will be required, unless the research plan changes significantly.
- If any of Qs 5-8 are answered Yes (Y), then approval from the Faculty Research Ethics Committee is required *before* the project can start. Approval can take over a month. Please consult with your supervisor about the process.

**Your supervisor must check your responses above *before* you submit this form.**

**Submit this completed form via the *Assignments* area in Blackboard (or elsewhere if so directed by the module leader or your supervisor).**

After you have uploaded, your supervisor will confirm that the checklist above has been correctly completed by marking this form as Passed/100% via the *My Grades* link on the Blackboard Welcome tab.

**If your submitted answers indicate that further ethical approval is indeed required, then you must also send this completed form to ResearchEthics@uwe.ac.uk**

Guidance is available at http://www1.uwe.ac.uk/research/researchethics.
Further guidance can be obtained via the module leader, in the first instance, or the Department's Faculty Research Ethics Committee representatives, including your department's *AHoD for Research*.